Noisy Homoclinic Pulse Dynamics

Tom Eaves

October 15, 2015

1 Near-homoclinic Pulse Dynamics

Near-homoclinic dynamics arise in a number of physically relevant problems in fluid dynamics, forexample, wherever there are coherent solitary waves, pulses in the signal of some important system variable, or bursts of turbulence in boundary layers. Near-homoclinic dynamics involve trajectories through phase space of a given dynamical system at parameter values close to a bifurcation at which there exits a homoclinic orbit, that repeatedly visit the vicinity of an unstable saddle point, at the origin say, followed by large excursions through the space, closely shadowing the saddle point's homoclinic orbit. If some variable like the energy or the distance from the saddle point is plotted against time, the resulting time series appears as a sequence of widely separated pulses.
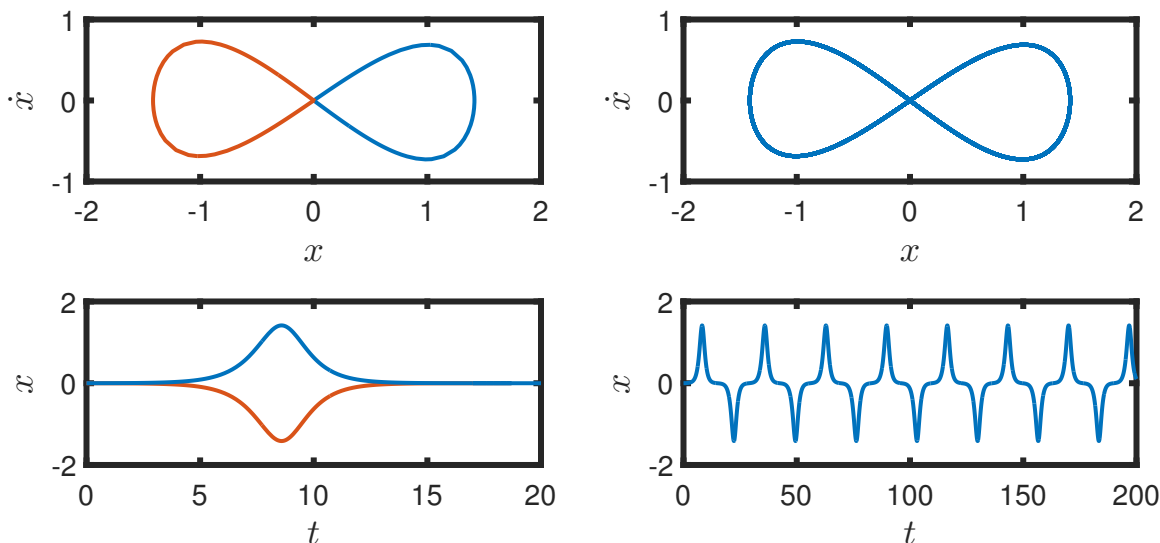

Figure 1: A deterministic two-dimensional system with a homoclinic orbit and its symmetric solution $x \mapsto -x$ (left) and a trajectory at nearby parameters (right). Top, trajectory in state space $(x(t), \dot{x}(t))$. Bottom, the homoclinic solution $x(t)$ and a sample train of pulses $x(t)$.

The exact form of such a 'pulse train' depends heavily on the type of saddle point that forms the start and end points of the homoclinic trajectory. In two dimensions, such

as the system plotted in Figure 1, both eigenvalues of the saddle point are real, and the time interval between pulses for the long-time asymptotic solution is constant. For a three-dimensional system like the Shimizu–Morioka system [14], which is a Lorenz-like system, for which the saddle point has three real eigenvalues $\lambda_2 < \lambda_1 < 0 < \lambda_3$, the strong contraction due to λ_2 can be ignored at leading order, and the dynamics appear at first sight to be similar to the two-dimensional case. However, the influence of the third stable direct acts to 'fold' trajectories together during their evolution through the vicinity of the origin, and chaotically distributed time intervals between pulses arises. The Shimizu–Morioka system is plotted in Figure 2.
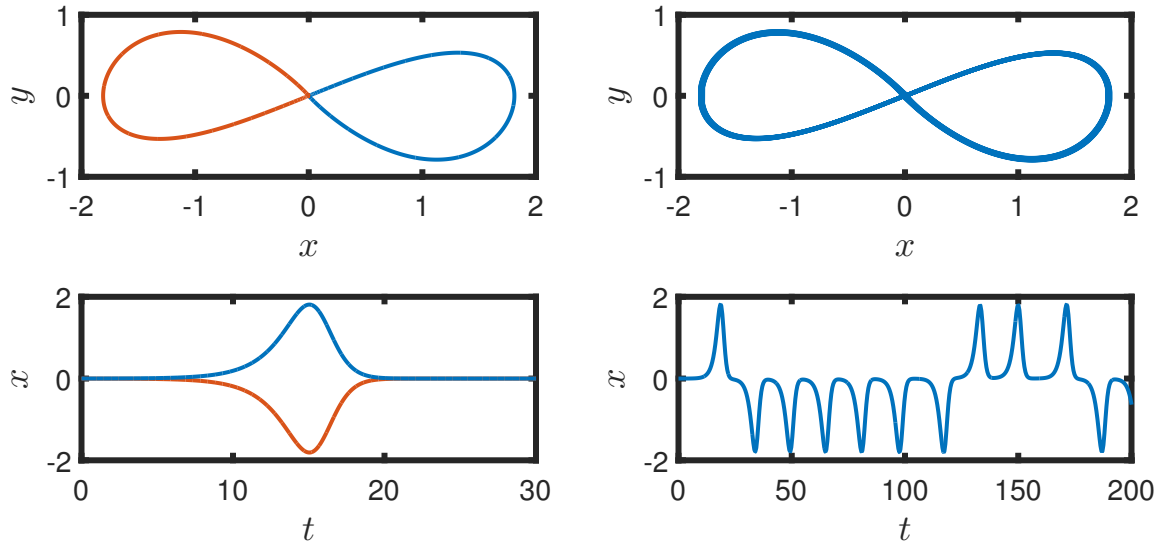

Figure 2: A deterministic three-dimensional Shimizu–Morioka system with a homoclinic orbit and its symmetric solution $(x, y) \mapsto (-x, -y)$ (left) and a trajectory at nearby parameters (right). Top, two-dimensional projection of trajectory in state space $(x(t), y(t))$. Bottom, the homoclinic solution $x(t)$ and a sample train of pulses $x(t)$..

Another canonical type of saddle point found in such systems is one for which the unstable direction has dimension one, and hence a single real positive eigenvalue, whilst the stable direction consists of a complex pair of eigenvalues. Their dynamics consist of trajectories spiraling into the saddle point before diverging away from the saddle point around its unstable direction. If this is combined with a strong contraction in one direction whilst following the homoclinic trajectory through state space, we call such systems 'Shilnikov' systems. These systems also display chaotically distributed time intervals between pulses, but in this case the chaos arises through the dynamics near the origin 'mixing up' trajectories that approach the origin through different locations, and thus completing a different number of spirals before leaving the vicinity of the saddle point. One such system is plotted in Figure 3.

Both Lorenz and Shilnikov type behaviour are observed in many physical systems. As was discussed in this year's GFD lectures by H. Dijkstra, the quasi-geostrophic double-gyre circulation undergoes bifurcations in an asymmetry variable, which measures the relative

occurrence of coherent structures above and below the symmetry line of forcing, to either Lorenz or Shilnikov phenomena, depending upon the parameters in the problem [9, 15].
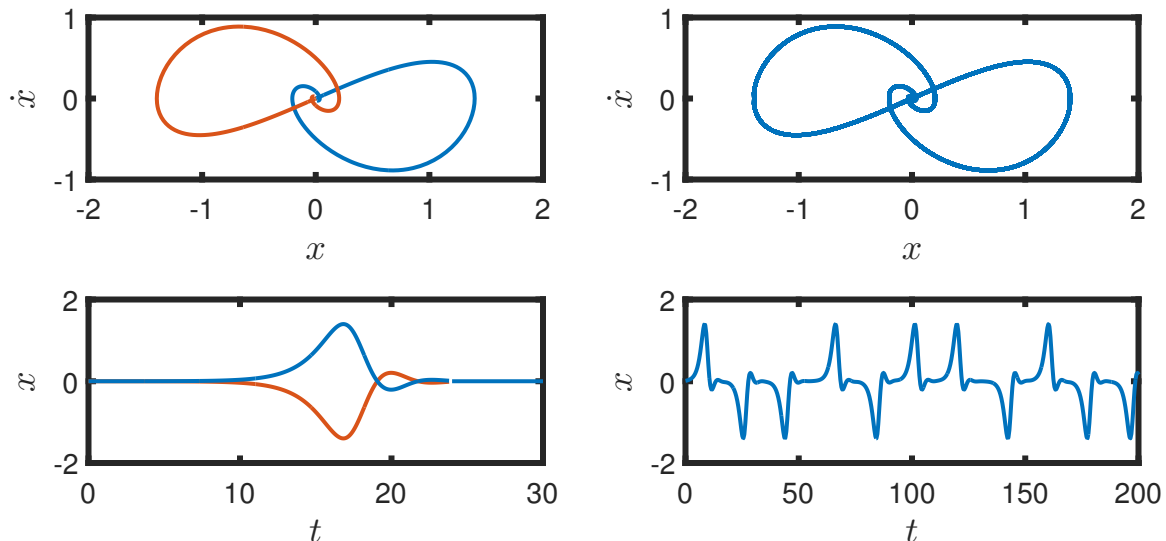

Figure 3: A deterministic three-dimensional Shilnikov system with a homoclinic orbit and its symmetric solution $x \mapsto -x$ (left) and a trajectory at nearby parameters (right). Top, two-dimensional projection of trajectory in state space $(x(t), \dot{x}(t))$. Bottom, the homoclinic solution $x(t)$ and a sample train of pulses $x(t)$.

The time intervals between pulses in all such systems depend most sensitively on how the trajectories evolve through the origin, as the closer a trajectory is to the stable manifold when approaching the origin, the longer it takes to leave the origin, and this time increases exponentially as the distance to the stable manifold decreases. In contrast, the 'outer' flow away from the origin takes an approximately constant time for all trajectories. The time intervals are therefore controlled by the position at which trajectories enter the vicinity of the origin.

Two successful approaches have been suggested to estimate the distribution of time intervals between pulses, or equivalently the mapping between trajectories leaving the origin and re-entering the origin. The approach taken by Shilnikov [13], after whom Shilnikov systems are named, is to solve the linearised system near the origin exactly, and to assume a linear mapping between points on a Poincaré section of trajectories leaving the origin to points on a Poincaré section of trajectories returning to the origin. This represents stong contraction in one of the spatial dimensions during the outer flow, and an outer flow that closely follows the homoclinic orbit, and is explained in more intuitive detail by Glendinning and Sparrow [7]. This can then be written as a single map between points on the entrance Poinaré section as

$$Z_{n+1} = C + B Z_n^\delta \cos\left(\Omega \log\left(\frac{Z_0}{Z_n}\right) + \Phi\right), \tag{1}$$

for some constant B, and C is a constant that measures the distance from a bifurcation point at which the homoclinic orbit exists, Φ is a constant phase, Ω is related to the unstable

eigenvalue and the imaginary part of the stable eigenvalue, and δ is the ratio of the real part of the stable eigenvalue to the unstable eigenvalue. When $C = 0$ and $\delta < 1$ this map has an infinite number of unstable fixed points, and exhibits chaos for most parameter values.

The approach taken by Balmforth *et al.* [4] and summarised a review paper [3], is to suppose that a solution to the equations in near homoclinic conditions can be written as a sum of homoclinic trajectories with an error term of $O(\epsilon)$, where ϵ measures the distance from homoclinicity. These homoclinic trajectories must then be sufficiently widely separated in time so that the interaction of adjacent homoclinic orbits is of size $O(\epsilon)$. An equation for the error term is derived, and a secularity condition deduced from the requirement that the error term is small. This secularity condition involves interactions of adjacent homoclinic trajectories, and hence can be interpreted as a mapping between successive spacings in time of the homoclinic trajectories. Under further approximation, this map can be reduced to the Shilnikov Z_n map. This method is the primary method generalised here to stochastic systems, and its details are left until later in the text.

Stochastic near-homoclinic systems have been considered in a variety of contexts, from noise-driven excitable systems [11, 5], to exponential tails in the timing of turbulence bursting events [18] and intermittent switching between cycles in a heteroclinic network [1]. The only major theoretical work comes from Stone and Holmes [17] and extensions [18, 16]. This work deals with the stochastic dynamics near the origin only, and solves the Ornstein–Uhlenbeck processes there, followed by assumptions of long residency time near the origin and small amplitude noise to find simple expressions for the density of points leaving and arriving at the origin, along with expected residency times. The key assumption in all of this work is that since the noise amplitude is small, its only significant effect is near to the origin, and that once a trajectory is closely following the homoclinic orbit away from the origin, the effects of noise can be neglected, and the distribution of points leaving the origin may be linearly mapped to a distribution of points arriving at the origin via the deterministic linear mapping, as in Shilnikov's approach for deterministic systems.

The work presented here demonstrates that this assumption is in fact unfounded, and we show that for the three different homoclinic systems discussed above, the primary effect of noise on a homoclinic trajectory is the influence during the orbit away from the origin producing a significant difference in the distribution of points arriving at the origin, and that this effect produces variances in the position and timing of trajectories that are at least an order of magnitude larger than the effects near the origin. Section 2 deals with the two-dimensional Duffing system originally considered in the theoretical paper of Stone and Holmes [17]. Section 3 deals with the three-dimensional Shimizu–Morioka system [14], which can be interpreted as the Lorenz system at high Rayleigh number and exhibits Lorenz-like behaviour. Section 4 deals with a three-dimensional equation that arises as the normal form of a co-dimension three bifurcation with a reflection symmetry [2] in which three eigenvalues of an equilibrium point simultaneously have zero real part, and exhibits Shilnikov-like behaviour. We draw our conclusions in Section 5.

2 A Stochastic Duffing Equation

Consider the following deterministic Duffing equation for $x(t)$

$$\ddot{x} = x - x^3 - \epsilon\gamma\dot{x} + \epsilon\beta x^2\dot{x}. \tag{2}$$

A sample trajectory with $\gamma = 0.08$ and $\beta = 0.1$ is shown in Figure 1, along with the nearby homoclinic trajectory at $\gamma \approx 0.080012$.

This equation has a fixed point at the origin, which is a saddle, with eigenvalues

$$\lambda = \frac{1}{2}(-\epsilon\gamma \pm \sqrt{\epsilon^2\gamma^2 + 4}) = \pm 1 - \frac{\epsilon\gamma}{2} + O(\epsilon^2), \tag{3}$$

with corresponding eigenvectors

$$\boldsymbol{v}_{\pm} = \begin{pmatrix} \pm 1 - \frac{\epsilon\gamma}{2} + O(\epsilon^2) \\ 1 \end{pmatrix}. \tag{4}$$

The system also has two addition fixed points at $(x, \dot{x}) = (\pm\sqrt{1 - \epsilon\gamma}, 0)$, which are unstable/stable sinks if $\beta \gtrless 0$.

Consider the addition of a white noise process to this equation, namely

$$\dot{x} = y + \epsilon\xi_x, \tag{5}$$
$$\dot{y} = x - x^3 - \epsilon\gamma y + \epsilon\beta x^2 y + \epsilon\xi_y, \tag{6}$$

where

$$\mathbb{E}(\xi_{x,y}(t)) = 0, \tag{7}$$
$$\mathbb{E}(\xi_{x,y}(t)\xi_{x,y}(s)) = \delta(t - s), \tag{8}$$

and ξ_x and ξ_y are independent.

Let δ be such that $\epsilon \ll \delta \ll 1$ and consider the small domain about the origin $\mathcal{D} = \{(x, \dot{x}) \cdot \hat{\boldsymbol{v}}_{\pm} \leq \delta\}$ where $\hat{\boldsymbol{v}}_{\pm}$ are the normalised eigenvectors of the saddle point at the origin. Within $\mathcal{D}$ we can approximate the dynamics, in local saddle coordinates, as

$$\dot{x}_1 = -\mu x_1 + \epsilon\xi_{x_1}, \tag{9}$$
$$\dot{x}_2 = \lambda x_2 + \epsilon\xi_{x_2}, \tag{10}$$

where $-\mu$ and λ are respectively the stable and unstable eigenvalues of the saddle point at the origin.

We can then consider three cases for the action of noise, namely

1. $\xi_{x_1} \neq 0$, $\xi_{x_2} \neq 0$ and $\xi = 0$ outside of $\mathcal{D}$ (noisy origin)

2. $\xi_{x_1} = 0$, $\xi_{x_2} = 0$ and $\xi \neq 0$ outside of $\mathcal{D}$ (deterministic origin)

3. $\xi_{x_1} \neq 0$, $\xi_{x_2} \neq 0$ and $\xi \neq 0$ outside of $\mathcal{D}$ (noise everywhere)

In addition, we may split case (1.) into two, namely $\xi_{x_1} \neq 0$ and $\xi_{x_2} = 0$ (noisy stable direction) and $\xi_{x_1} = 0$ and $\xi_{x_2} \neq 0$ (noisy unstable direction). This is done in Appendix A.

Before considering each of the three cases in turn, we first solve the deterministic behaviour within $\mathcal{D}$.
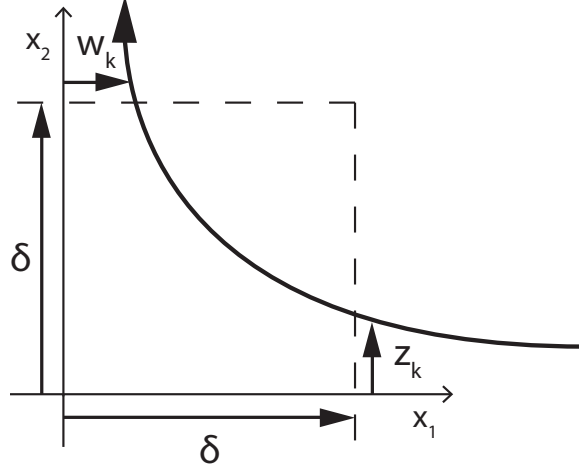
Figure 4: Sketch of the dynamics through the domain $\mathcal{D}$ about the origin with entry point z_k and leaving point w_k.

2.1 Deterministic origin dynamics

When a trajectory enters $\mathcal{D}$ for the kth occasion, at time $t = t_0$, we have $(x_1, x_2) = (\delta, z_k)$, see Figure 4. The trajectory then satisfies

$$x_1 = \delta e^{-\mu(t-t_0)}, \tag{11}$$

$$x_2 = z_k e^{\lambda(t-t_0)}. \tag{12}$$

The trajectory then leaves $\mathcal{D}$ when $(x_1, x_2) = (w_k, \delta)$, which occurs after a time interval

$$t_k \equiv t_{\text{leave}} - t_0 = \frac{1}{\lambda} \log\left(\frac{\delta}{z_k}\right), \tag{13}$$

from which we can obtain w_n, the x_1 position at time of exit,

$$w_k = \delta^{1-\mu/\lambda} z_k^{\mu/\lambda}. \tag{14}$$

We then make the assumption that the dynamics outside of $\mathcal{D}$ act as a linear mapping between the point at which $\mathcal{D}$ is left for the kth time to the point at which $\mathcal{D}$ is entered for the $(k+1)$th time, as did Shilnikov [13], i.e. that

$$z_{k+1} = \alpha w_k + c = \alpha \delta^{1-\mu/\lambda} z_k^{\mu/\lambda} + c, \tag{15}$$

where $c = 0$ when there exists a homoclinic orbit.

Since $z_k < \delta < 1$, we see that when $\mu/\lambda > 1$, we have the limit $z_k \to c$ as $k \to \infty$. We can also solve for the time intervals between entering events. First note that

$$t_{k+1} = -\frac{1}{\lambda} \log\left(\frac{z_{k+1}}{\delta}\right) = -\frac{1}{\lambda} \log(\alpha \delta^{-\mu/\lambda} z_k^{\mu/\lambda} + c/\delta) = -\frac{1}{\lambda} \log(\alpha e^{-\mu t_k} + c/\delta). \tag{16}$$

Assuming that the time between exit and re-entrance of $\mathcal{D}$ is T, the time interval between entering events $\Delta_k = T + t_k$ satisfies

$$\Delta_{k+1} = T - \frac{1}{\lambda} \log(\alpha e^{-\mu \Delta_k} e^{\mu T} + c/\delta). \tag{17}$$

When there exists a homoclinic orbit, $c = 0$, and so

$$\Delta_{k+1} = T - \frac{\log(\alpha)}{\lambda} - \frac{\mu T}{\lambda} + \frac{\mu}{\lambda} \Delta_k, \tag{18}$$

and so if $\mu/\lambda > 1$, we have the limit $\Delta_k \to \infty$ as $n \to \infty$, and so the homoclinic orbit is attracting.

2.2 Noisy origin, $\xi = 0$ outside $\mathcal{D}$

The analysis in this section is a summary of the work of Stone and Holmes [17] and their approach to determining the dynamics for noise near the origin. In Appendix A we adopt the same approach as Stone and Holmes to investigate the effect of noise near the origin only in either the stable or unstable direction of the saddle. We wish to solve the stochastic differential equations

$$\dot{x}_1 = -\mu x_1 + \epsilon \xi_{x_1}, \tag{19}$$

$$\dot{x}_2 = \lambda x_2 + \epsilon \xi_{x_2}, \tag{20}$$

where λ and $-\mu$ are the unstable and stable eigenvalues at the origin.

First, we define the Gaussian function for the normal probability density function

$$\mathcal{N}_x(a, \sigma^2) \equiv \frac{1}{\sqrt{2\pi\sigma^2}} \exp\left[-\frac{(x-a)^2}{2\sigma^2}\right]. \tag{21}$$

Then, the known solutions to the Ornstein–Uhlenbeck processes (19-20), given an initial known position are

$$\rho(x_1, t|\delta, 0) = \mathcal{N}_{x_1}\left(\delta e^{-\mu t}, \frac{\epsilon^2}{2\mu}(1 - e^{-2\mu t})\right) \tag{22}$$

$$\rho(x_2, t|z_n, 0) = \mathcal{N}_{x_2}\left(z_k e^{\lambda t}, \frac{\epsilon^2}{2\lambda}(e^{2\lambda t} - 1)\right) \tag{23}$$

Observe that the means satisfy the equations

$$\frac{\mathrm{d}}{\mathrm{d}t}\langle x_1 \rangle = -\mu\langle x_1 \rangle \tag{24}$$

$$\frac{\mathrm{d}}{\mathrm{d}t}\langle x_2 \rangle = \lambda\langle x_2 \rangle, \tag{25}$$

and so we might expect that if the deterministic system spends a large amount of time in $\mathcal{D}$, then so will the stochastic system. This allows us to make the approximation that the x_1-process becomes stationary before exiting $\mathcal{D}$, i.e. that $e^{-\mu t} \ll 1$, and so we have

$$\rho(x_1, t|\delta, 0) \sim \mathcal{N}\left(0, \frac{\epsilon^2}{2\mu}\right) \quad \text{as } t \to \infty, \tag{26}$$

and so the leaving point w_k has a distribution independent of z_k,

$$\rho(w_k) = \mathcal{N}\left(0, \frac{\epsilon^2}{2\mu}\right). \tag{27}$$

After leaving $\mathcal{D}$, the motion is deterministic, and so we recall the linear mapping

$$z_{k+1} = \alpha w_k + c, \tag{28}$$

giving the density of return points z_{k+1},

$$\rho(z_{k+1}|z_k) = \rho(z_{k+1}) = \mathcal{N}\left(c, \frac{\epsilon^2 \alpha^2}{2\mu}\right), \tag{29}$$

using standard results for linear combinations of normally distributed random variables.

To find the timings t_k, we need to solve the unstable Y process. It is also known that the solution to the Ornstein–Uhlenbeck process (20) given an initial known *normal distribution* is

$$\rho(x_2, t|\mathcal{N}(x_2^0, \sigma^2), 0) = \mathcal{N}\left(x_2^0 e^{\lambda t}, \sigma^2 e^{2\lambda t} + \frac{\epsilon^2}{2\lambda}(e^{2\lambda t} - 1)\right), \tag{30}$$

and so, we see that

$$\rho\left(x_2, t\left|\mathcal{N}\left(ce^{\lambda t}, \frac{\epsilon^2 \alpha^2}{2\mu}\right), 0\right.\right) = \mathcal{N}\left(ce^{\lambda t}, \frac{\epsilon^2 \alpha^2}{2\mu}e^{2\lambda t} + \frac{\epsilon^2}{2\lambda}(e^{2\lambda t} - 1)\right) \tag{31}$$

$$= \mathcal{N}\left(ce^{\lambda t}, \frac{\epsilon^2}{2\lambda}(e^{2\lambda s} - 1)\right) \tag{32}$$

$$\equiv \rho(x_2, s|s = 0), \tag{33}$$

where $s = t + t'$ and

$$t' = \frac{1}{2\lambda}\log\left(1 + \frac{\alpha^2 \lambda}{\mu}\right). \tag{34}$$

Then, the mean passage time $\mathbb{E}(t_k)$ satisfies

$$\mathbb{E}(t_k) = \int_0^\infty \mathbb{P}(t_k > t) \, \mathrm{d}t \tag{35}$$

$$= \int_{t'}^\infty \mathbb{P}(t_k > s) \, \mathrm{d}s \tag{36}$$

$$= \int_{t'}^\infty \int_{-\delta}^\delta \rho(x_2, s|s = 0) \, \mathrm{d}x_2 \, \mathrm{d}s \tag{37}$$

$$\sim \begin{cases} \frac{1}{\lambda}\log\left(\frac{\delta}{\epsilon}\right) & \text{for } c \ll \epsilon \ll \delta \ll 1, \\ \frac{1}{\lambda}\log\left(\frac{\delta}{c}\right) & \text{for } \epsilon \ll c \ll \delta \ll 1. \end{cases} \tag{38}$$

The main result here is that for nearly homoclinic conditions in which $c \ll \epsilon$, noise acts to effectively push a trajectory away from the stable axis to a distance ϵ, after which the mean trajectory is essentially deterministic, whereas far from homoclinicity in which $\epsilon \ll c$, noise is unimportant, and the mean trajectory is identical to its deterministic version. The

extra condition that $\epsilon, c \ll \delta$ ensures that trajectories remain in $\mathcal{D}$ for a long time, and so the assumption $e^{-\mu t_k} \ll 1$ is valid.

Parameter values considered by Stone and Holmes [17] are $\gamma = 0.08$, $\beta = 0.1$ and $\epsilon = 0.0006$. Using these values, we can compare the results above to a numerical solution of the stochastic differential equations with $\xi = 0$ outside of $\mathcal{D}$, defined by $\delta = 0.1$. Figure 5 shows a comparison of the distributions for $\rho(w_k)$ and the distributions for $\rho(z_k)$ for both a numerical integration of the SDEs and the derived results (27,29) given by Stone and Holmes [17] with $c = 0$. There is a clear discrepancy in these results, and so we also plot the sum of two normal distributions with means $\pm\delta \exp(-\mu\mathbb{E}(t_k))$ for w_n where $\mathbb{E}(t_n)$ is taken from the numerical integration, and an approximate offset $c = \pm 2.763 \times 10^{-4}$ for z_n taken from the numerical integration. The mean time through $\mathcal{D}$ for the numerical solution is 5.767 and the mean time according to (38) with $c \ll \epsilon$ is 5.325. There remains an error in the comparison of the results for $\rho(w_k)$, likely due to the fact that the approximation for $\rho(w_k)$ is independent of z_k.

We note that we can break from the approach of Stone and Holmes in this section and Appendix A. Rather than making approximation about long residency times to simplify the relevant probability densities, we can instead keep the exact solutions to the Ornstein–Uhlenbeck processes and iteratively produce a sample trajectory. To obtain z_{k+1} from z_k, we choose a t_k and w_k from the relevant densities, and then map w_k to z_{k+1} using the linear mapping assumption. This would give a reliable, if low-tech way of producing the correct comparisons to the SDEs.
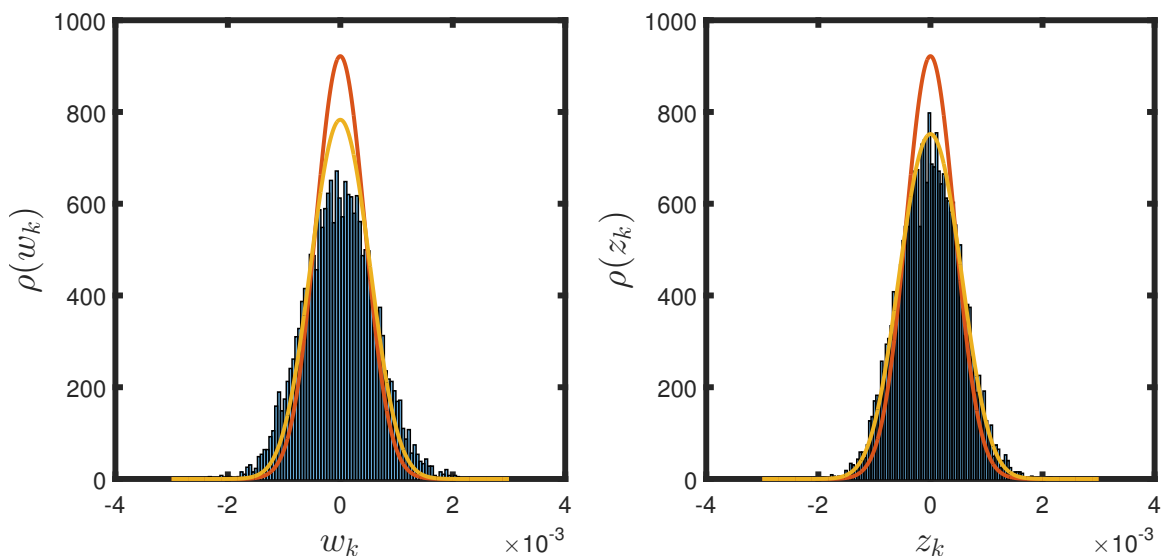

Figure 5: Probability density of leave points w_n (left) and return (right) points z_n to $\mathcal{D}$ with $\delta = 0.1$ and noise strength $\epsilon = 0.0006$ acting only outside $\mathcal{D}$, for parameters $\gamma = 0.08$ and $\beta = 0.1$ for a direct numerical simulation with 7500 returns to $\mathcal{D}$ (blue histogram), the approximate solution (27,29) from Stone and Holmes [17] (red line), and the sum of two normal distributions with means $\pm\delta \exp(-\mu\mathbb{E}(t_n))$ for w_n and $\pm 2.763 \times 10^{-4}$ for z_n (orange line).

2.3 Deterministic origin, $\xi \neq 0$ outside $\mathcal{D}$

Consider the equation

$$\ddot{x} = x - x^3 - \epsilon\gamma\dot{x} + \epsilon\beta x^2\dot{x} + \epsilon\xi(t) \tag{39}$$

outside the domain $\mathcal{D} \approx \{|\dot{x}+x| \leq \delta, \ |\dot{x}-x| \leq \delta\}$. Write the solution as $x = x_0 + \epsilon x_1 + O(\epsilon^2)$. Then, at $O(1)$ we have

$$\ddot{x}_0 = x_0 - x_0^3, \tag{40}$$

which has first integral

$$\frac{1}{2}\dot{x}_0^2 = \frac{1}{2}x_0^2 - \frac{1}{4}x_0^4 + E, \tag{41}$$

where we can interpret the constant of integration E as an energy parameter. The case $E = 0$ gives the homoclinic orbits

$$x_0 = \pm\sqrt{2}\,\mathrm{sech}(t - t_0) \tag{42}$$

for some t_0. We will concentrate on the positive solution, $x_0 = \sqrt{2}\,\mathrm{sech}(t - t_0)$.

Next, at $O(\epsilon)$ we obtain

$$\ddot{x}_1 - x_1 + 3x_0^2 x_1 = -\gamma\dot{x}_0 + \beta x_0^2\dot{x}_0 + \xi(t). \tag{43}$$

Multiply through by $\dot{x}_0$ and integrate to get

$$\left[\dot{x}_0\dot{x}_1 - x_0 x_1 + x_0^3 x_1\right]_{t_a}^{t_b} = -\gamma \int_{t_a}^{t_b} \dot{x}_0^2 \ \mathrm{d}t + \beta \int_{t_a}^{t_b} x_0^2\dot{x}_0^2 \ \mathrm{d}t + \int_{t_a}^{t_b} \xi(t)\dot{x}_0 \ \mathrm{d}t, \tag{44}$$

where t_a and t_b are defined respectively by

$$\dot{x} + x = \sqrt{2}\delta, \tag{45}$$
$$\dot{x} - x = -\sqrt{2}\delta. \tag{46}$$

For $\epsilon \ll \delta \ll 1$, we have $x_0 \approx 2\sqrt{2}e^{-|\hat{t}|}$, where $\hat{t} = t - t_0$. This then gives $\dot{x}_0 \approx -2\sqrt{2}\,\mathrm{sgn}(\hat{t})e^{-|\hat{t}|}$, and so the leading order condition on $\partial\mathcal{D}$ determines t_a and t_b, namely

$$\dot{x}_0(t_a) = x_0(t_a) = \frac{\sqrt{2}\delta}{2}, \tag{47}$$

$$\dot{x}_0(t_b) = -x_0(t_b) = -\frac{\sqrt{2}\delta}{2}, \tag{48}$$

$$t_b = -t_a = \log\left(\frac{4}{\delta}\right). \tag{49}$$

At second order we obtain

$$\dot{x}_1(t_a) = -x_1(t_a), \tag{50}$$
$$\dot{x}_1(t_b) = x_1(t_b), \tag{51}$$

and so

$$\left[\dot{x}_0\dot{x}_1 - x_0 x_1 + x_0^3 x_1\right]_{t_a}^{t_b} = \sqrt{2}\delta(x_1(t_a) - x_1(t_b)) + O(\delta^3). \tag{52}$$

We also have the exact relations

$$-\gamma \int_{-\infty}^{\infty} \dot{x}_0^2 = -\frac{4\gamma}{3}, \tag{53}$$

$$\beta \int_{-\infty}^{\infty} x_0^2 \dot{x}_0^2 \, dt = \frac{16\beta}{15}, \tag{54}$$

and so, given that $-t_a, t_b \gg 1$, the deterministic orbit is homoclinic at leading order if these two integrals are equal, i.e. $\beta = 5\gamma/4$. Assuming homoclinic conditions, we obtain

$$\sqrt{2}\delta(x_1(t_a) - x_1(t_b)) = \int_{-\infty}^{\infty} \xi(t)\dot{x}_0 \, dt. \tag{55}$$

It is a known result [6] that for deterministic functions of time $f(t)$,

$$\int_a^b f(t)\xi(t) \, dt \sim \mathcal{N}\left(0, \int_a^b f(t)^2 \, dt\right). \tag{56}$$

We can use this result to deduce that

$$x_1(t_b) \sim \mathcal{N}\left(x_1(t_a), \frac{1}{2\delta^2} \int_{-\infty}^{\infty} \dot{x}_0^2 \, dt\right) \tag{57}$$

$$= \mathcal{N}\left(x_1(t_a), \frac{2}{3\delta^2}\right). \tag{58}$$

The leading order return map to $\mathcal{D}$ for this stochastic Duffing equation in homoclinic conditions is then,

$$z_{k+1} = \left.\frac{\dot{x} + x}{\sqrt{2}}\right|_{t_b} \tag{59}$$

$$= \sqrt{2}\epsilon x_1(t_b) \tag{60}$$

$$= \mathcal{N}\left(\sqrt{2}\epsilon x_1(t_a), \frac{4\epsilon^2}{3\delta^2}\right) \tag{61}$$

$$= \mathcal{N}\left(w_k, \frac{4\epsilon^2}{3\delta^2}\right) \tag{62}$$

$$= \text{sgn}(z_k)\delta^{1-\mu/\lambda}|z_k|^{\mu/\lambda} + \frac{\epsilon}{\delta}\sqrt{\frac{4}{3}}\eta_k, \tag{63}$$

where $\eta_k \sim \mathcal{N}(0, 1)$ is a zero mean, unit variance, Gaussian random variable. Hence,

$$m = \mathbb{E}(z_{k+1}|z_k) = \text{sgn}(z_k)\delta^{1-\mu/\lambda}|z_n|^{\mu/\lambda} \tag{64}$$

$$\mathbb{E}((z_{k+1} - m)^2|z_k) = \frac{4\epsilon^2}{3\delta^2}. \tag{65}$$

Recall that the variance in the re-entry point for noise only within $\mathcal{D}$ scaled as ϵ^2. Given $\epsilon \ll \delta \ll 1$, we see that the variance associated with this outer flow is much larger.

We then have the transition density

$$\rho(z_{k+1}|z_k) = \mathcal{N}\left(\text{sgn}(z_k)\delta^{1-\mu/\lambda}|z_k|^{\mu/\lambda}, \frac{4\epsilon^2}{3\delta^2}\right), \tag{66}$$

and so

$$\rho(z_{k+1}) = \int_{-\infty}^{\infty} \rho(z_{k+1}|z_k)\rho(z_k)\mathrm{d}z_k. \tag{67}$$

We can look for the stationary distribution $\rho(z_k) = \rho^s(z)$ that the mapping approaches as $n \to \infty$. This is given by the integral equation

$$\rho^s(z) = \int_{-\infty}^{\infty} \frac{\delta}{\epsilon}\sqrt{\frac{3}{8\pi}} \exp\left[-\frac{3\delta^2(z - \text{sgn}(s)\delta^{1-\mu/\lambda}|s|^{\mu/\lambda})^2}{8\epsilon^2}\right]\rho^s(s) \, \mathrm{d}s. \tag{68}$$

Figure 6 shows the return distribution for noise outside of $\mathcal{D}$ only and noise uniformly everywhere in the system respectively. Also shown is the mapping (63). For noise outside of $\mathcal{D}$ we also plot the estimated stationary distribution via the method described below, and for the 'noise everywhere' calculation we also plot the result from Stone and Holmes.
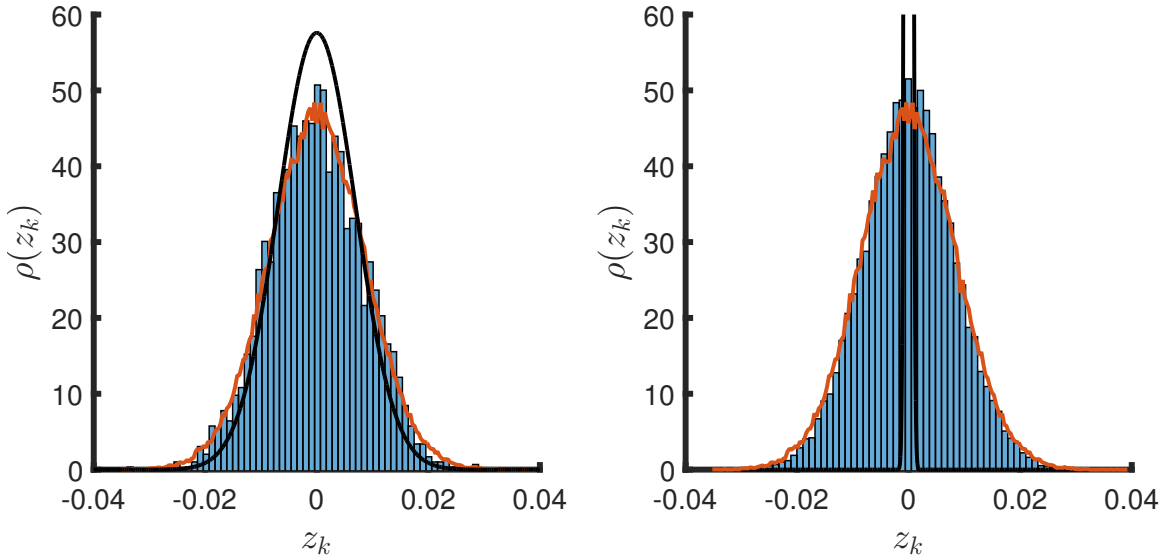

Figure 6: Left: Probability density of return points to $\mathcal{D}$ with $\delta = 0.1$ and noise strength $\epsilon = 0.0006$ acting only outside $\mathcal{D}$, for parameters $\gamma = 0.08$ and $\beta = 0.1$ for a direct numerical simulation with 3000 returns to $\mathcal{D}$ (blue histogram), the return map (63) iterated 10^5 times (red line) and the asymptotic approximation to the stationary distribution of the return map (63) (black line). Right: Noise strength $\epsilon = 0.0006$ acting everywhere, and the result of Stone and Holmes [17] (black line).

Before computing additional properties of this solution, we need some results about stationary distributions about stable fixed points of maps.

2.4 Weak noise estimation of stationary distributions

We can estimate stationary distributions for stochastic mappings with stable deterministic fixed points or periodic orbits [10]. Suppose that we have the stochatic mapping

$$z_{n+1} = f(z_n) + \epsilon \eta_n, \tag{69}$$

where $\eta_n \sim \mathcal{N}(0,1)$. Then we know that

$$\rho(z_{n+1}|z_n) = \mathcal{N}(f(z_n), \epsilon^2), \tag{70}$$

and so the stationary distribution statisfies

$$\rho^s(z) = \int \rho(z|s)\rho^s(s) \; \mathrm{d}s. \tag{71}$$

Suppose in addition that (for the simplest possible case) the deterministic part of the mapping has a singe stable fixed point, $f(z_*) = z_*$ with $|f'_*| \equiv |f'(z_*)| < 1$. Then we might suppose that for small noise strength ϵ, the stationary distribution is centred about z_* with some variance σ^2 which in general is different from, but related to, ϵ, and should depend on the local rate of contraction of $f(z)$ about the fixed point.

To this end, try the ansatz

$$\rho^s(z) = \frac{1}{\sqrt{2\pi\sigma^2}} \exp\left[-\frac{(z-z_*)^2}{2\sigma^2}\right] \tag{72}$$

$$= \int \frac{1}{2\pi\epsilon\sigma} \exp\left[-\frac{(z-f(s))^2}{2\epsilon^2} - \frac{(s-z_*)^2}{2\sigma^2}\right] \mathrm{d}s \tag{73}$$

Now let $s = z_* + \epsilon S$ and $z = z_* + \epsilon Z = f(z_*) + \epsilon Z$. Then, defining $\alpha^2 = \epsilon^2/\sigma^2$, we obtain

$$\rho^s(z) = \int \frac{1}{2\pi\sigma} \exp\left[-\frac{(Z - f'_* S)^2}{2} - \frac{\alpha^2 S^2}{2}\right] \mathrm{d}S \tag{74}$$

$$\equiv \int \frac{1}{2\pi\sigma} \exp(\phi(S)) \; \mathrm{d}S. \tag{75}$$

Now, the function $\phi(S)$ has a minima at

$$S = S_0 = \frac{f'_*}{\alpha^2 + f'^2_*} Z, \tag{76}$$

and we may approximate

$$\phi(S) = \phi(S_0) + \frac{(S-S_0)^2}{2}\phi''(S) \tag{77}$$

$$= -\frac{\alpha^2}{\alpha^2 + f'^2_*}\frac{Z^2}{2} - (f'^2_* + \alpha^2)\frac{(S-S_0)^2}{2}. \tag{78}$$

Substituting this back into the integral and evaluating the resulting Gaussian, we obtain

$$\rho^s(z) = \frac{1}{2\pi\sigma} \sqrt{\frac{2\pi}{f_*'^2 + \alpha^2}} \exp\left[-\frac{\alpha^2}{\alpha^2 + f_*'^2} \frac{Z^2}{2}\right] \tag{79}$$

$$= \frac{1}{\sqrt{2\pi\sigma^2(f_*'^2 + \alpha^2)}} \exp\left[-\frac{\alpha^2}{\alpha^2 + f_*'^2} \frac{(z - z_*)^2}{2\epsilon^2}\right], \tag{80}$$

which is consistent with the original ansatz if $\sigma^2 = \epsilon^2/(1 - f_*'^2)$, and this modified variance σ^2 is positive provided that the fixed point is stable. Hence, an approximate solution is

$$\rho^s(z) = \frac{1}{\sqrt{2\pi\epsilon^2/(1 - f_*'^2)}} \exp\left[-\frac{(z - z_*)^2}{2\epsilon^2/(1 - f_*'^2)}\right]. \tag{81}$$

Now consider a stable N-cycle $\{z_i\}_{i=1}^N$ distinct points with $f(z_i) = z_{i+1}$. Define $f_i' = f'(z_i)$. Then, we pose the ansatz for the stationary distribution

$$\rho^s(z) = \sum_{i=1}^N \frac{a_i}{\sqrt{2\pi\sigma_i^2}} \exp\left[-\frac{(z - z_i)^2}{2\sigma_i^2}\right], \tag{82}$$

with $a_i > 0$ and $\sum a_i = 1$ so that this represents a probability distribution. An analogous calculation to the one above gives

$$\rho^s(z) = \sum_{i=1}^N \frac{a_i}{\sqrt{2\pi\sigma_i^2(f_i'^2 + \alpha^2)}} \exp\left[-\frac{\alpha_i^2}{\alpha_i^2 + f_i'^2} \frac{(z - z_i)^2}{2\epsilon^2}\right], \tag{83}$$

where $\alpha_i^2 = \epsilon^2/\sigma_i^2$.

One of the compatibility conditions gives $a_i = a_{i+1}$, and so $a_i = 1/N$. The other compatibility condition gives

$$\sigma_i^2 = \epsilon^2 \frac{1 + \sum_{k=1}^{N-1} \prod_{j=1}^k f_{i-j}'^2}{1 - \prod_{j=1}^N f_j'^2}, \tag{84}$$

where the subscripts are taken modulo N, which reduces to the fixed point case if $N = 1$.

For the Duffing equation considered above in homoclinic conditions, we have $z_* = 0$ and $f_*' = 0$, and so the estimated variance of the stationary distribution is the same as that for the noise term in the equation. This estimate is plotted in Figure 6 along with the numerical simulation of the full system, and the map iterated a large number of times (10^5). The agreement is not particularly good, but this is due to the fact that $z_* \neq 0$ for the parameter values chosen by Stone and Holmes [17]. We fix this later.

2.5 Timing map for deterministic origin, $\xi \neq 0$ outside $\mathcal{D}$

We can also compute the time between pulses, or equivalently the time between re-entries of $\mathcal{D}$. The total flight time is the sum of the time taken to pass through the origin plus the time taken between leaving and returning to $\mathcal{D}$,

$$\Delta_n = T_{\text{origin}} + T_{flight} = \frac{1}{\lambda} \log\left(\frac{\delta}{|z_n|}\right) + 2t_b = \frac{1}{\lambda} \log\left(\frac{\delta}{|z_n|}\right) + 2 \log\left(\frac{4}{\delta}\right). \tag{85}$$

The timing map should then be independent of δ. Substituting Δ_n into the return map (63) we obtain

$$e^{-\lambda\Delta_{n+1}} = \delta^{2(\lambda-\mu)}16^{\mu-\lambda}e^{-\mu\Delta_n} + \frac{\delta^{2\lambda-2}\epsilon}{16^\lambda}\sqrt{\frac{4}{3}}\eta_n \tag{86}$$

$$= e^{-\mu\Delta_n} + \frac{\epsilon}{16}\sqrt{\frac{4}{3}}\eta_n, \tag{87}$$

at leading order, since $\lambda, \mu = 1 \pm \epsilon\gamma/2$, and so δ drops out. Note however that we must keep λ and μ different from one in the exponentials as contraction is necessary for bounded solutions. This can be seen be noting that if $\lambda = \mu = 1$ in the return map (63), then z_n satisfies a Wiener process with variance growing linearly with the number of iterations.

We can also demonstrate that the timing map has exponential tails. To see this, recall that the return map (63) has a stable fixed point at $z_n = 0$ and so the approximations of the previous section imply that we have the stationary distribution

$$\rho_z(z) \approx \mathcal{N}\left(0, \frac{4\epsilon^2}{3\delta^2}\right). \tag{88}$$

Then, the change of variables to Δ gives

$$\rho_\Delta(\Delta) \approx 16\lambda\sqrt{\frac{3}{2\pi}}\frac{\delta^{2-2\lambda}e^{-\lambda\Delta}}{\epsilon}\exp\left[-\delta^{4-4\lambda}\frac{96}{\epsilon^2}e^{-2\lambda\Delta}\right] \tag{89}$$

$$\approx 16\lambda\sqrt{\frac{3}{2\pi}}\frac{e^{-\lambda\Delta}}{\epsilon}\exp\left[-\frac{96}{\epsilon^2}e^{-2\lambda\Delta}\right] \tag{90}$$

$$\sim 16\lambda\sqrt{\frac{3}{2\pi}}\frac{e^{-\lambda\Delta}}{\epsilon} \quad \text{as } \Delta \to \infty \tag{91}$$

In Figure 7 we plot the distribution of the times between maxima for the same numerical simulation as for the return points plotted in 6 along with the estimate above, both with and without making the approximation $\delta^{1-\lambda} = 1$. In each case the exponential decay is correct, but the density without the assumption is more accurate. This is likely due to the fact that for these parameter values, λ and μ are in fact significantly different from one. Additionally, for this range of λ and μ, the excursion time away from the origin is not quite $2\log(4/\delta)$, providing an additional source of error. All of these approximation are fixed in the next section, where we generalise the homoclinic pulse expansion technique of ODE of Balmforth *et al.* [4] to stochastic systems.

In addition, we can estimate the expected time between maxima as

$$\mathbb{E}(\Delta) \approx \int_0^\infty 16\lambda\sqrt{\frac{3}{2\pi}}\frac{\Delta e^{-\lambda\Delta}}{\epsilon}\exp\left[-\frac{96}{\epsilon^2}e^{-2\lambda\Delta}\right]\,\mathrm{d}\Delta \tag{92}$$

$$= \int_0^{\sqrt{96}/\epsilon} 16\sqrt{\frac{3}{2\pi}}\frac{1}{\sqrt{96}\lambda}\log\left(\frac{\sqrt{96}}{\epsilon s}\right)e^{-s^2}\,\mathrm{d}s \tag{93}$$

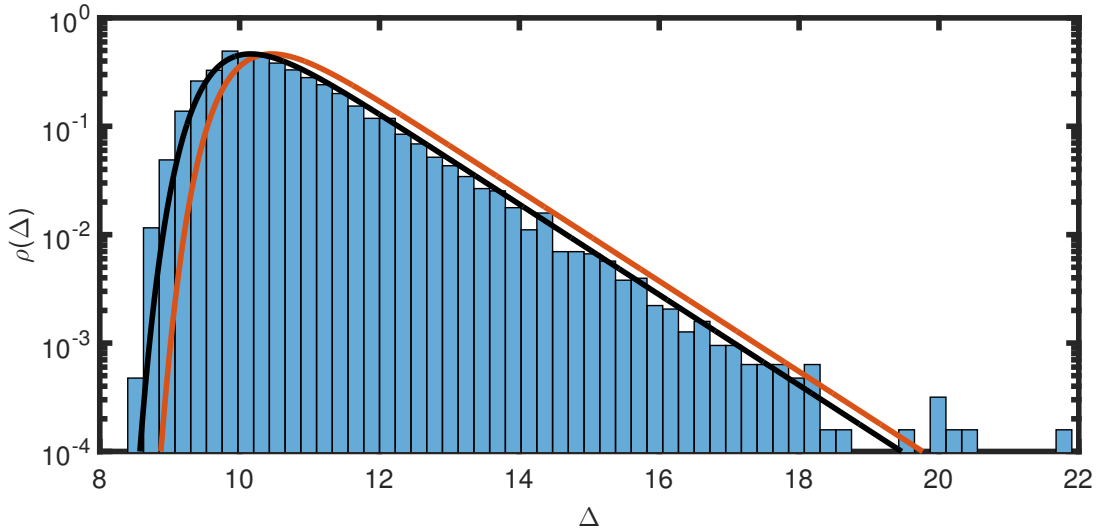$$\sim \frac{1}{\lambda}\log\left(\frac{\sqrt{96}}{\epsilon}\right) \quad \text{as } \epsilon \to 0. \tag{94}$$

Figure 7: Probability density of times between maxima to with noise strength $\epsilon = 0.0006$ acting only outside $\mathcal{D}$, for parameters $\gamma = 0.08$ and $\beta = 0.1$ for a direct numerical simulation with 3000 returns to $\mathcal{D}$ (blue histogram), the estimated solution with $\delta^{1-\lambda} = 1$ (red line) and the estimated solution with $\delta^{1-\lambda} \neq 1$ (black line).

For the numerical data shown in Figure 7 we have $\mathbb{E}(\Delta) = 10.695$, and the formula above with $\epsilon = 0.0006$ gives $\mathbb{E}(\Delta) = 10.097$. To compare to the work of Stone and Holmes, recall that the mean time through the origin was

$$\mathbb{E}(t_n) = \frac{1}{\lambda} \log\left(\frac{\delta}{\epsilon}\right), \tag{95}$$

and so the mean flight time is

$$\tau = \mathbb{E}(t_n) + 2t_b \tag{96}$$

$$= \frac{1}{\lambda} \log\left(\frac{\delta}{\epsilon}\right) + 2\log\left(\frac{4}{\delta}\right) \tag{97}$$

$$= \frac{1}{\lambda} \log\left(\frac{\delta^{1-2\lambda}4^{2\lambda}}{\epsilon}\right) \tag{98}$$

$$\approx \frac{1}{\lambda} \log\left(\frac{16}{\epsilon\delta}\right), \tag{99}$$

which, in addition to depending explicitly on δ, takes the value 13.003 for the parameters used here, which is clearly not a good approximation.

2.6 Homoclinic pulse expansion for the stochastic Duffing system

To move away from the assumption that $\gamma, \beta = O(\epsilon)$, and to correct the discrepancy with the timing map distribution requiring $\delta^{1-\lambda} = 1$, consider the equation

$$\ddot{x} - x + x^3 + \gamma\dot{x} - \beta x^2 \dot{x} = \epsilon\sigma\xi(t). \tag{100}$$

Let $\gamma = \gamma_0(\beta)$ be the parameter set for which there exists a homoclinic orbit, and write $\gamma = \gamma_0 + \epsilon\gamma_1$. To consider $\xi \neq 0$ *everywhere*, we instead make the ansatz for the full solution as

$$x(t) = \sum_k \theta_k H(t - t_k) + \epsilon R \equiv \sum \theta_k H_k + \epsilon R, \tag{101}$$

where $H(t)$ is the homoclinic solution, the sequence of times $\{t_k\}$ are sufficiently widely seperated so that $H_k H_{k\pm1} = O(\epsilon)$, the polarity $\theta_k = \pm 1$ accounts for the symmetry $x \mapsto -x$, and ϵR is the error made in making this assumption. This is the singular perturbation method for finding timing between homoclinic pulses of ODEs of Balmforth *et al.* [4], but here we can generalise it to stochastic systems.

In order to begin the asymptotic expansion, we need to explain what is meant by $O(\epsilon)$ interaction of neighbouring homoclinic orbits. Most importantly, we need to have an expansion for the nonlinear terms in (100). For correctly chosen times $\{t_k\}$ we have

$$\left(\sum_k \theta_k H_k \right)^3 = \sum_k \theta_k H_k^3 + 3 \sum_k H_k^2 (\theta_{k+1} H_{k+1} + \theta_{k-1} H_{k-1}) + O(\epsilon^2), \tag{102}$$

for the cubic term, where the second term is $O(\epsilon)$. The term $\beta x^2 \dot{x}$ may be treated similarly.

The $O(\epsilon^0)$ equation is satisfied automatically, and the $O(\epsilon)$ equation in the vicinity of t_k gives

$$\mathcal{J}_k R = -\frac{3}{\epsilon} H_k^2 (\theta_{k+1} H_{k+1} + \theta_{k-1} H_{k-1}) + \frac{\beta}{\epsilon} \frac{\mathrm{d}}{\mathrm{d}t} [H_k^2 (\theta_{k+1} H_{k+1} + \theta_{k-1} H_{k-1})] + \sigma\xi - \gamma_1 \theta_k \dot{H}_k \tag{103}$$

for each k, where

$$\mathcal{J}_k = \mathcal{L} + 3H_k^2 - \beta \frac{\mathrm{d}}{\mathrm{d}t} H_k^2. \tag{104}$$

We note that the correct operator acting on R should involved the sum over all k to include all pulses, but we note that this sum is highly peaked about each homlinic trajectory, and so we may approximate by splitting the sum up, and requiring R to satisfy a simpler equation for each k. The error made in this approximation is of higher order in ϵ and so we employ it here [4].

Next, define $N_k \neq 0$ by

$$\mathcal{J}_k^\dagger N_k = 0. \tag{105}$$

Then, multiply through by N_k and integrate to obtain

$$0 = \int_{-\infty}^{\infty} N_k \left[-\frac{3}{\epsilon} H_k^2 (\theta_{k+1} H_{k+1} + \theta_{k-1} H_{k-1}) \right.$$
$$\left. + \frac{\beta}{\epsilon} \frac{\mathrm{d}}{\mathrm{d}t} [H_k^2 (\theta_{k+1} H_{k+1} + \theta_{k-1} H_{k-1})] + \sigma\xi - \gamma_1 \theta_k H_k \right] \mathrm{d}t \tag{106}$$

$$= \int_{-\infty}^{\infty} \left[-\frac{3N_k + \beta \dot{N}_k}{\epsilon} H_k^2 (\theta_{k+1} H_{k+1} + \theta_{k-1} H_{k-1}) + N_k (\sigma\xi - \gamma_1 \theta_k \dot{H}_k) \right] \mathrm{d}t \tag{107}$$

We have that

$$H_{k-1} \sim h_\infty e^{\mu(t - t_{k-1})} \quad \text{as } t - t_{k-1} \to \infty \tag{108}$$

$$H_{k+1} \sim h_0 e^{\lambda(t - t_{k+1})} \quad \text{as } t - t_{k+1} \to -\infty, \tag{109}$$

and so although strictly speaking we should only integrate the equations over the k-th pulse, we can approximate the neighbouring pulses in the integral, and integrate over the whole real line and obtain

$$\int_{-\infty}^{\infty} (3N_k + \beta \dot{N}_k) H_k^2 H_{k+1} \, \mathrm{d}t \approx \int_{-\infty}^{\infty} (3N_k + \beta \dot{N}_k) H_k^2 h_0 e^{\lambda(t - t_{k+1})} \, \mathrm{d}t \tag{110}$$

$$= h_0 e^{-\lambda(t_{k+1} - t_k)} \int_{-\infty}^{\infty} (3N_k + \beta \dot{N}_k) H_k^2 e^{\lambda(t - t_k)} \, \mathrm{d}t \tag{111}$$

$$= h_0 e^{-\lambda(t_{k+1} - t_k)} \int_{-\infty}^{\infty} (3N + \beta \dot{N}) H^2 e^{\lambda t} \, \mathrm{d}t \tag{112}$$

$$\equiv A e^{-\lambda \Delta_{k+1}}, \tag{113}$$

where $\Delta_k = t_k - t_{k-1}$, and similarly,

$$\int_{-\infty}^{\infty} (3N_k + \beta \dot{N}_k) H_k^2 H_{k-1} \, \mathrm{d}t \approx h_\infty e^{-\mu(t_k - t_{k-1})} \int_{-\infty}^{\infty} (3N + \beta \dot{N}) H^2 e^{-\mu t} \, \mathrm{d}t \equiv B e^{-\mu \Delta_k}. \tag{114}$$

We are then left with the timing map

$$\theta_{k+1} e^{-\lambda \Delta_{k+1}} = \theta_k \epsilon C + \theta_{k-1} D e^{-\mu \Delta_k} + \epsilon \sigma M \eta_k, \tag{115}$$

where $\eta_k \sim \mathcal{N}(0,1)$, $C = -C_0/A$, $D = -B/A$, $M = -M_0/A$, and

$$C_0 = \int_{-\infty}^{\infty} \gamma_1 N \dot{H} \, \mathrm{d}t \tag{116}$$

$$M_0^2 = \int_{-\infty}^{\infty} N^2 \mathrm{d}t. \tag{117}$$

We can convert the timing map (115) into a return-like map through the change of variables $z_k = \theta_k \theta_{k-1} \exp(-\lambda \Delta_k)$, which gives

$$z_{k+1} = \epsilon C + \mathrm{sgn}(z_k) D |z_k|^{\mu/\lambda} + \epsilon \sigma M \eta_k. \tag{118}$$

For small ϵ this equation has a deterministic fixed point $z = z_* = O(\epsilon)$ with $0 < |f'_*| \lesssim O(1)$ when λ and μ are not far from one. Hence, we can approximate the stationary distribution for z_k by

$$\rho_{z_k}(z) = \frac{1}{\sqrt{2\pi \epsilon^2 \sigma^2 M^2 / (1 - f'^2_*)}} \exp\left[-\frac{(z - z_*)^2}{2\epsilon^2 \sigma^2 M^2 / (1 - f'^2_*)} \right], \tag{119}$$

and so the stationary distribution for the timings Δ_k is given approximately by

$$\rho_{\Delta_k}(\Delta) = \frac{\lambda e^{-\lambda \Delta}}{\sqrt{2\pi \epsilon^2 \sigma^2 M^2 / (1 - f'^2_*)}} \left(\exp\left[-\frac{(e^{-\lambda \Delta} - z_*)^2}{2\epsilon^2 \sigma^2 M^2 / (1 - f'^2_*)} \right] \right.$$

$$\left. + \exp\left[-\frac{(e^{-\lambda \Delta} + z_*)^2}{2\epsilon^2 \sigma^2 M^2 / (1 - f'^2_*)} \right] \right) \tag{120}$$

$$\sim \frac{2\lambda e^{-\lambda \Delta}}{\sqrt{2\pi \epsilon^2 \sigma^2 M^2 / (1 - f'^2_*)}} \exp\left[-\frac{z_*^2}{2\epsilon^2 \sigma^2 M^2 / (1 - f'^2_*)} \right] \quad \text{as } \Delta \to \infty, \tag{121}$$

and so we obtain an exponential decay of the timing probability density function.

For the parameters $\gamma = 0.08$ and $\beta = 0.01$ with noise strength $\epsilon\sigma = 0.0006$, as used by Stone and Holmes [17], we have $\epsilon C = -1.362 \times 10^{-6}$ with fixed point $z_* = -2.576 \times 10^{-6}$ and $f'_* = 0.511$. Figure 8 shows the estimated densities $\rho_z(z)$ and $\rho_\Delta(\Delta)$ respectively, along with a numerical iteration of the timing map (115).
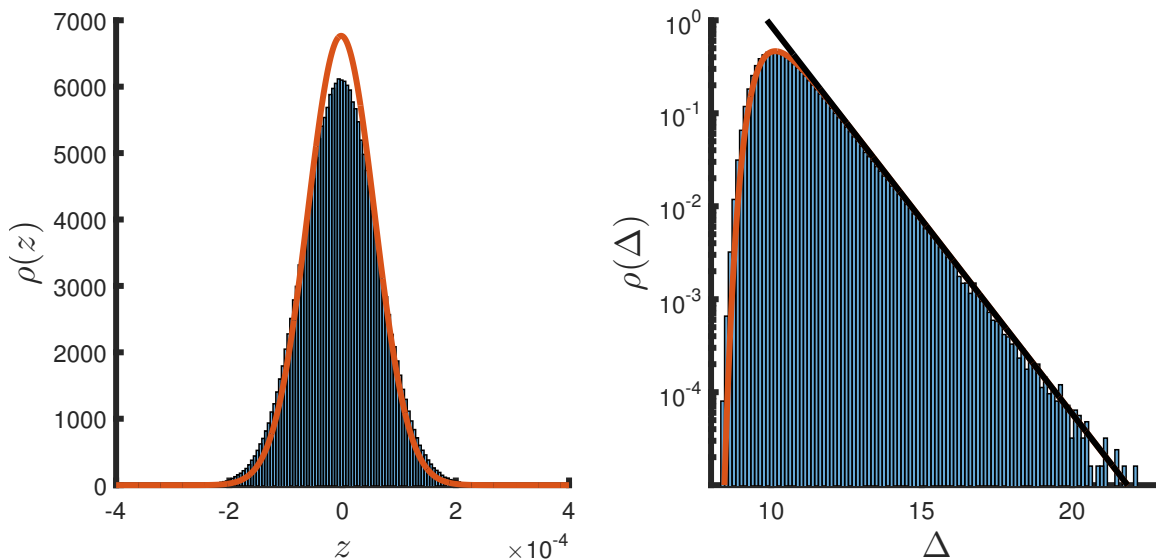

Figure 8: Left: Probability density of z_k, for parameters $\gamma = 0.08$ and $\beta = 0.1$ with noise strength $\epsilon\sigma = 0.0006$ for the derived asymptotic map (blue histogram), and the estimated solution with (red line). Right: Probability density of Δ_n, for parameters $\gamma = 0.08$ and $\beta = 0.1$ with noise strength $\epsilon\sigma = 0.0006$ for the derived asymptotic map (blue histogram), the estimated solution with (red line), and its large Δ exponential decay (black line).

We can also approximate the mean spacing $\mathbb{E}(\Delta)$ from

$$\mathbb{E}(\Delta) = \int_0^\infty \Delta \rho_{\Delta_k}(\Delta) \, \mathrm{d}\Delta, \tag{122}$$

which takes different forms in the two cases $|z_*| \ll a \ll 1$ and $a \ll |z_*| \ll 1$, where

$$a^2 = \epsilon^2 \sigma^2 M^2 / (1 - f'^2_*), \tag{123}$$

which is the effective variance of the z_n stationary distribution.

First, we look at $a \ll |z_*| \ll 1$, which we would expect to correspond to the case where noise is not strong enough to change $\mathbb{E}(\Delta)$ from its deterministic value. We have that the first exponential in the integral for $\mathbb{E}(\Delta)$ takes its maximum at $y = e^{-\lambda\Delta} = z_*$, which is well separated from the lower limit of integration, and the second exponential is asymptotically small. Hence,

$$\mathbb{E}(\Delta) \sim \frac{1}{\sqrt{2\pi a^2}} \frac{1}{\lambda} \log\left(\frac{1}{z_*}\right) \int_{-\infty}^\infty e^{-(y-z_*)^2/2a^2} \, \mathrm{d}y \tag{124}$$

$$= \frac{1}{\lambda} \log\left(\frac{1}{z_*}\right), \tag{125}$$

which is the deterministic value, as expected.

Next, for $|z_*| \ll a \ll 1$, we expect that the fixed point z_* does not greatly influence $\mathbb{E}(\Delta)$, and that the mean spacing should depend instead on a. In this limit, the two exponentials are comparible, and we may set $z_* = 0$ (though not $f_*'^2 = f_0'^2 = 0$), so that a remains unchanged. We then obtain

$$\mathbb{E}(\Delta) \sim \frac{2}{\sqrt{2\pi a^2}} \int_0^1 \frac{1}{\lambda} \log\left(\frac{1}{y}\right) e^{-y^2/2a^2} \, dy \tag{126}$$

$$\sim \frac{2}{\sqrt{\pi}} \int_0^\infty \frac{1}{\lambda} \log\left(\frac{1}{as\sqrt{2}}\right) e^{-s^2} \, ds \tag{127}$$

$$= \frac{1}{\lambda} \log\left(\frac{1}{a}\right) + \frac{1}{2\lambda}(\gamma_e + \log 2) \tag{128}$$

$$\sim \frac{1}{\lambda} \log\left(\frac{1}{a}\right), \tag{129}$$

where γ_e is Euler's gamma constant.

Figure 9 shows the mean spacing $\mathbb{E}(\Delta)$ as a function of noise strength $\epsilon\sigma$ for the parameters $\gamma = 0.08$ and $\beta = 0.1$, for the timing map (115) and the original stochastic differential equation. Also plotted are the two asymptotic estimates above, for $a \ll |z_*| \ll 1$ and $|z_*| \ll a$. For the second case, $|z_*| \ll a$, we have $(\gamma_e + \log(2))/2\lambda \approx 0.661$, which is around 5% of the typical mean spacing in this range. For this reason, we plot both the leading order asymptotic result, and its correction. It is clear that the first correction is needed in this case. There are also plotted dashed lines at the two locations $\sigma\epsilon = z_*$ and $a = a(\epsilon\sigma) = z_*$. A first guess might be that the transition in behaviour occurs when the strength of the noise $\epsilon\sigma$ is comparable with z_*, but we have shown above that it is in fact the effective noise strength a that controls the change in behaviour. The figure clearly shows this.

We see also in Figure 9 that the asymptotic approximation (129) begins to break down as $\epsilon\sigma$ increases from 10^{-3}. This is to be expected eventually since we require $a(\epsilon) \ll 1$ for the Laplace approximation of the integral for $\mathbb{E}(\Delta)$ to be valid. Additionally, as $\mathbb{E}(\Delta)$ decreases, it eventually approaches the flight time taken along the homoclinic orbit, and so the assumption of well spaced pulses breaks down.

This generalised homoclinic pulse expansion technique has is clearly able to accurately reproduce the results of the full stochastic differential equations. In stark contrast to the results of Stone and Holmes [17], we have been able to fully characterise the effect of noise on the system. It is clear that the results for the noise away from the origin problem and the noise everywhere case are essentially the same and the the noise near the origin case of Stone and Holmes is significantly different (see Figures 6 and 8). The dynamics can be reduced to a simple stochastic one dimensional map of the form $z_{k+1} = f(z_k) + \sigma\eta_k$ which can be interpreted as the system obeying the deterministic dynamics $f(z_k)$ except for a random 'kick' upon re-entry to the origin, which depends on the sensitivity of the homoclinic solution to noise perturbations along its whole length. The system is controlled most closely by this kick upon re-entry, and is a fully nonlinear phenomena of the coupling between noise and nonlinear dynamics.

In the following sections we use the same technique to investigate the two other homoclinic systems, and find in each case the simple reduction to a stochastic mapping of the same form.
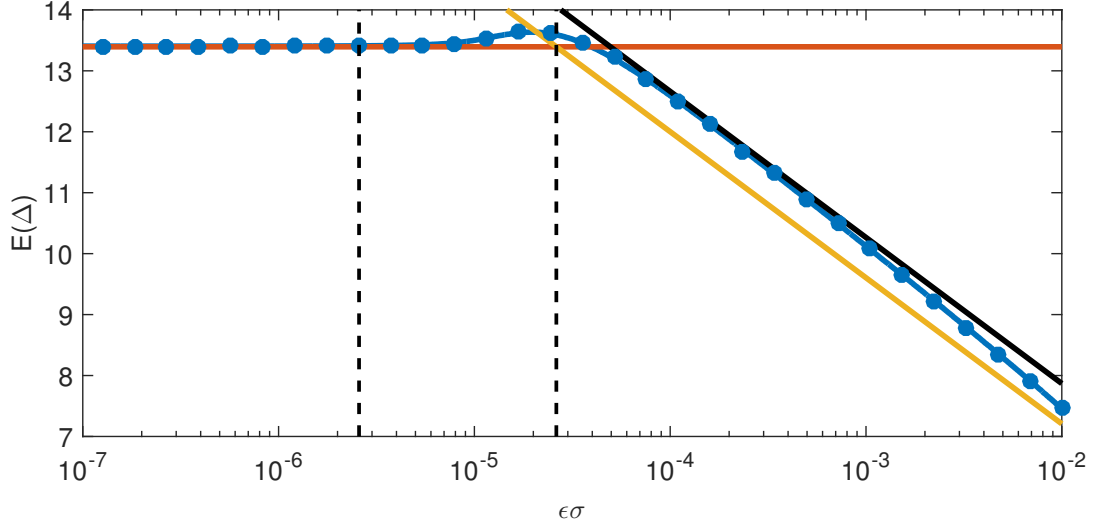
Figure 9: Mean spacing $\mathbb{E}(\Delta)$ as a function of noise strength $\epsilon\sigma$, for parameters $\gamma = 0.08$ and $\beta = 0.1$ for the derived asymptotic map (blue line), and the original stochastic differential equation (blue dots). Also plotted is the asymptotic result for $a \ll |z_*| \ll 1$ (red line), the leading asymptotic result for $|z_*| \ll a$ (orange line) and its correction (solid black line). The leftmost dashed line shows $\epsilon\sigma = z_*$ and the rightmost dashed line shows $a = a(\epsilon\sigma) = z_*$.

3 Stochastic Shimizu–Murayama Model

The deterministic Shimizu–Murayama system [14] models the Lorenz equations at high Rayleigh number, and for a range of parameters exhibits near homoclinic behaviour [12]. The three-dimensional stochastic system is

$$\dot{x} = y + \epsilon\sigma\xi_x \tag{130}$$
$$\dot{y} = x(1 - z) - \lambda y + \epsilon\sigma\xi_y \tag{131}$$
$$\dot{z} = -\alpha(z - x^2) + \epsilon\sigma\xi_z, \tag{132}$$

or equivalently,

$$\frac{\mathrm{d}}{\mathrm{d}t}\boldsymbol{x} = A\boldsymbol{x} + \boldsymbol{f}(\boldsymbol{x}) + \epsilon\sigma\boldsymbol{\xi}, \tag{133}$$

where $\boldsymbol{x} = (x, y, z)$, $\boldsymbol{\xi} = (\xi_x, \xi_y, \xi_z)$, the matrix A is

$$A = \begin{pmatrix} 0 & 1 & 0 \\ 1 & -\lambda & 0 \\ 0 & 0 & -\alpha \end{pmatrix} = \begin{pmatrix} 0 & 1 & 0 \\ 1 & -\lambda_0 & 0 \\ 0 & 0 & -\alpha \end{pmatrix} + \epsilon \begin{pmatrix} 0 & 0 & 0 \\ 0 & -\lambda_1 & 0 \\ 0 & 0 & 0 \end{pmatrix} \equiv A_0 + \epsilon A_1, \tag{134}$$

where $\lambda = \lambda_0 + \epsilon\lambda_1$ and $\lambda_0(\alpha)$ are the parameter values at which there is a homoclinic orbit, and the vector $\boldsymbol{f}(\boldsymbol{x})$ is

$$\boldsymbol{f}(\boldsymbol{x}) = \begin{pmatrix} 0 \\ -xz \\ \alpha x^2 \end{pmatrix}. \tag{135}$$

We will consider cases with $\alpha, \lambda > 0$. A sample trajectory with $\alpha = 0.4$ and $\lambda = 1.1954$ is shown in Figure 2 along with its nearby homoclinic orbit at $\lambda \approx 1.2054$.

This system has fixed points at $(0, 0, 0)$ and $(\pm 1, 0, 1)$. The second of these is either a stable sink or unstable source. We are interested in the cases for which the origin is a saddle with two stable directions and one unstable directions. The eigenvalues and eigenvectors at the origin are

$$-\alpha \; : \; \begin{pmatrix} 0 \\ 0 \\ 1 \end{pmatrix} \quad \text{stable,} \tag{136}$$

$$-\mu_- = (-\lambda - \sqrt{4 + \lambda^2})/2 \; : \; \begin{pmatrix} (\lambda - \sqrt{4 + \lambda^2})/2 \\ 1 \\ 0 \end{pmatrix} \quad \text{stable,} \tag{137}$$

$$\mu_+ = (-\lambda + \sqrt{4 + \lambda^2})/2 \; : \; \begin{pmatrix} (\lambda + \sqrt{4 + \lambda^2})/2 \\ 1 \\ 0 \end{pmatrix} \quad \text{unstable.} \tag{138}$$

Let $\boldsymbol{H} = (H^x, H^y, H^z)$ be the homoclinic orbit that leaves the origin with $x > 0$. This system has the symmetry $(x, y, z) \mapsto (-x, -y, z)$, and so define $\phi \boldsymbol{H} = (\theta H^x, \theta H^y, H^z)$ for the polarity $\theta = \pm 1$. We then pose a solution of the form

$$\boldsymbol{x} = \sum_k \phi_k \boldsymbol{H}_k + \epsilon \boldsymbol{R}, \tag{139}$$

where $\boldsymbol{H}_k = \boldsymbol{H}(t - t_k)$ and the times t_k are well-separated so that $\boldsymbol{H}_k \cdot \boldsymbol{H}_{k \pm 1} = O(\epsilon)$. Then, at $O(\epsilon^0)$ we find the homoclinic solution, and at $O(\epsilon)$ we obtain

$$\mathcal{L}_{\phi_k} \boldsymbol{R} = \frac{1}{\epsilon} \boldsymbol{f}'(\phi_k \boldsymbol{H}_k) \cdot (\phi_{k+1} \boldsymbol{H}_{k+1} + \phi_{k-1} \boldsymbol{H}_{k-1}) + A_1 \boldsymbol{H}_k + \sigma \boldsymbol{\xi}, \tag{140}$$

where

$$\mathcal{L}_{\phi_k} = \frac{\mathrm{d}}{\mathrm{d}t} - A_0 - \boldsymbol{f}'(\phi_k \boldsymbol{H}_k), \tag{141}$$

and

$$\boldsymbol{f}'(\phi \boldsymbol{H}) = \begin{pmatrix} 0 & 0 & 0 \\ -H^z & 0 & -\theta H^x \\ 2\alpha\theta H^x & 0 & 0 \end{pmatrix} \tag{142}$$

is the Jacobian matrix of the nonlinear part of the differential equations.

Now define $\mathcal{L}_{\phi_k}^\dagger$ by

$$\mathcal{L}_{\phi_k}^\dagger = -\frac{\mathrm{d}}{\mathrm{d}t} - A_0^\dagger - \boldsymbol{f}'(\phi_k \boldsymbol{H}_k)^\dagger, \tag{143}$$

and define $\boldsymbol{N}_{\phi_k} \neq 0$ by

$$\mathcal{L}_{\phi_k}^\dagger \boldsymbol{N}_{\phi_k} = 0. \tag{144}$$

Note that the equation satisfied by $\boldsymbol{N}_-$ is related to that satisfied by $\boldsymbol{N}_+$ through a symmetry, so that if $\boldsymbol{N}_+ = (N^x, N^y, N^z)$, then $\boldsymbol{N}_- = (N^x, N^y, -N^z)$. To this end, write instead $\boldsymbol{N}_{\phi_k} = \psi_k \boldsymbol{N}_k = (N_k^x, N_k^y, \theta_k N_k^z)$ and $\boldsymbol{N}_k$ satisfies

$$\mathcal{L}_{+(k)}^\dagger \boldsymbol{N}_k = 0. \tag{145}$$

Now we may take the dot product of the equation satisfied by $\boldsymbol{R}$ with $\psi_k \boldsymbol{N}_k$ and integrate to obtain

$$0 = \int \left[\frac{1}{\epsilon} \psi_k \boldsymbol{N}_k \cdot \boldsymbol{f}'(\phi_k \boldsymbol{H}_k) \cdot (\phi_{k+1} \boldsymbol{H}_{k+1} + \phi_{k-1} \boldsymbol{H}_{k-1}) + \psi_k \boldsymbol{N}_k \cdot (A_1 \phi_k \boldsymbol{H}_k + \sigma \boldsymbol{\xi}) \right] \, \mathrm{d}t. \tag{146}$$

In order to estimate the interaction integrals, we note that

$$\boldsymbol{H} \sim \begin{pmatrix} h_0^x \\ h_0^y \\ 0 \end{pmatrix} e^{\mu_+ t} \quad \text{as } t \to -\infty \tag{147}$$

$$\boldsymbol{H} \sim \begin{pmatrix} h_\infty^x \\ h_\infty^y \\ 0 \end{pmatrix} e^{-\mu_- t} + \begin{pmatrix} 0 \\ 0 \\ h_\infty^z \end{pmatrix} e^{-\alpha t} \quad \text{as } t \to \infty, \tag{148}$$

but $\mu_- > \alpha$ and so we may approximate

$$\boldsymbol{H} \sim \begin{pmatrix} 0 \\ 0 \\ h_\infty^z \end{pmatrix} e^{-\alpha t} \quad \text{as } t \to \infty, \tag{149}$$

which is equivalent to assuming a strong contraction in one of the stable directions, and so trajectories essentially become two-dimensional when passing nearby to the origin.

We may now approximate each of the interaction integrals to obtain

$$\int \psi_k \boldsymbol{N}_k \cdot \boldsymbol{f}'(\phi_k \boldsymbol{H}_k) \cdot \phi_{k+1} \boldsymbol{H}_{k+1} \, \mathrm{d}t \tag{150}$$

$$= \int \begin{pmatrix} N_k^x \\ N_k^y \\ \theta_k N_k^z \end{pmatrix} \cdot \begin{pmatrix} 0 & 0 & 0 \\ -H_k^z & 0 & -\theta_k H_k^x \\ 2\alpha \theta_k H_k^x & 0 & 0 \end{pmatrix} \cdot \begin{pmatrix} \theta_{k+1} h_0^x \\ \theta_{k+1} h_0^y \\ 0 \end{pmatrix} e^{\mu_+(t - t_{k+1})} \, \mathrm{d}t \tag{151}$$

$$= h_0^x e^{-\mu_+(t_{k+1} - t_k)} \theta_{k+1} \int (2\alpha H^x N^z - H^z N^y) e^{\mu_+ t} \, \mathrm{d}t \tag{152}$$

$$\equiv \theta_{k+1} e^{-\mu_+ \Delta_{k+1}} A, \tag{153}$$

where $\Delta_k = t_k - t_{k-1}$, and similarly,

$$\int \psi_k \boldsymbol{N}_k \cdot \boldsymbol{f}'(\phi_k \boldsymbol{H}_k) \cdot \phi_{k-1} \boldsymbol{H}_{k-1} \, \mathrm{d}t \tag{154}$$

$$= -h_\infty^z e^{-\alpha(t_k - t_{k-1})} \theta_k \int H^x N^y e^{-\alpha t} \, \mathrm{d}t \tag{155}$$

$$\equiv -\theta_k e^{-\alpha \Delta_k} B_0. \tag{156}$$

Putting this together, we obtain the timing map

$$\theta_{k+1} e^{-\mu_+ \Delta_{k+1}} = \epsilon \theta_k C + \theta_k B e^{-\alpha \Delta_k} + \epsilon \sigma M \eta_k, \tag{157}$$

where $\eta_k \sim \mathcal{N}(0,1)$ and $B = B_0/A$, $C = C_0/A$ and $M = M_0/A$, where

$$C_0 = \int \lambda_1 N^y H^y \, \mathrm{d}t, \tag{158}$$

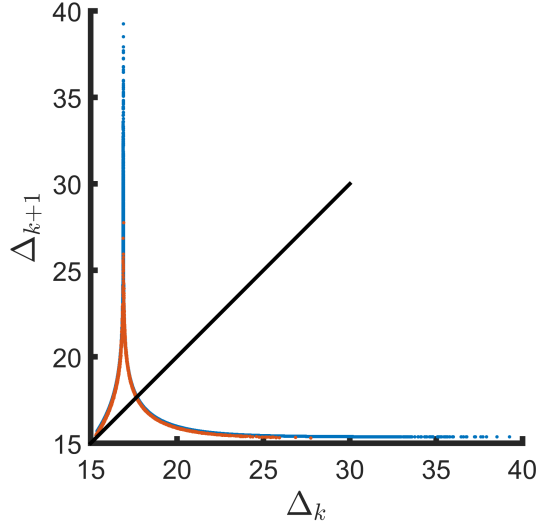$$M_0^2 = \int \boldsymbol{N} \cdot \boldsymbol{N} \, \mathrm{d}t. \tag{159}$$

Figure 10: Timings for the Shimizu–Morioka system with no noise, $\sigma = 0$, and parameters $\alpha = 0.4$ and $\lambda = 1.1954$. Numerical simulation (red), and iterates of the derived timing map (blue).

Figure 10 shows a comparison between the above timing map and a numerical simulation of the system for no noise, $\sigma = 0$, $\alpha = 0.4$ and $\lambda = 1.1954$. The agreement is very good, and so we now concentrate only on the map, rather than the numerical simulations.

Figure 11 shows iterations of the derived timing map for noise strengths $\epsilon\sigma = 0$, 10^{-4}, 10^{-3} and 4×10^{-3} with $\alpha = 0.4$ and $\lambda = 1.1954$. We see that as the noise strength is increased, the deterministic structure is gradually broadened and smoothed out, before eventually being destroyed altogether. However, the shape of the probability distributions is largely unchanged, and are similar to the Duffing distributions for all noise strengths, as shown in Figure 12. Only at large noise strengths is there an appreciable shift in the peak of the distribution and a broadening of the tails.

4 A Stochastic Shilnikov System

Consider the ODE

$$\dddot{x} + \gamma\ddot{x} + \dot{x} - cx + x^3 = 0, \tag{160}$$

which is the normal form of a co-dimension three bifurcation [2] with the symmetry $x \mapsto -x$. Consider a stochastic equivalent of this equation

$$\dddot{x} + \gamma\ddot{x} + \dot{x} - cx + x^3 + \epsilon\sigma\xi(t) = 0, \tag{161}$$
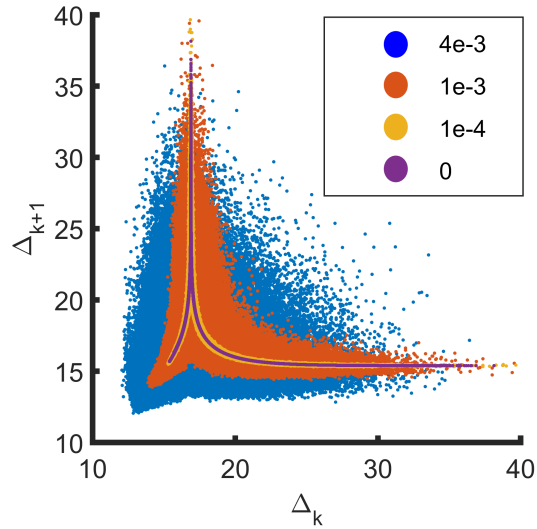
Figure 11: Timings for the Shimizu–Morioka system calculated from the derived map with noise strengths $\epsilon\sigma = 0$, 10^{-4}, 10^{-3} and 4×10^{-3} for parameters $\alpha = 0.4$ and $\lambda = 1.1954$.
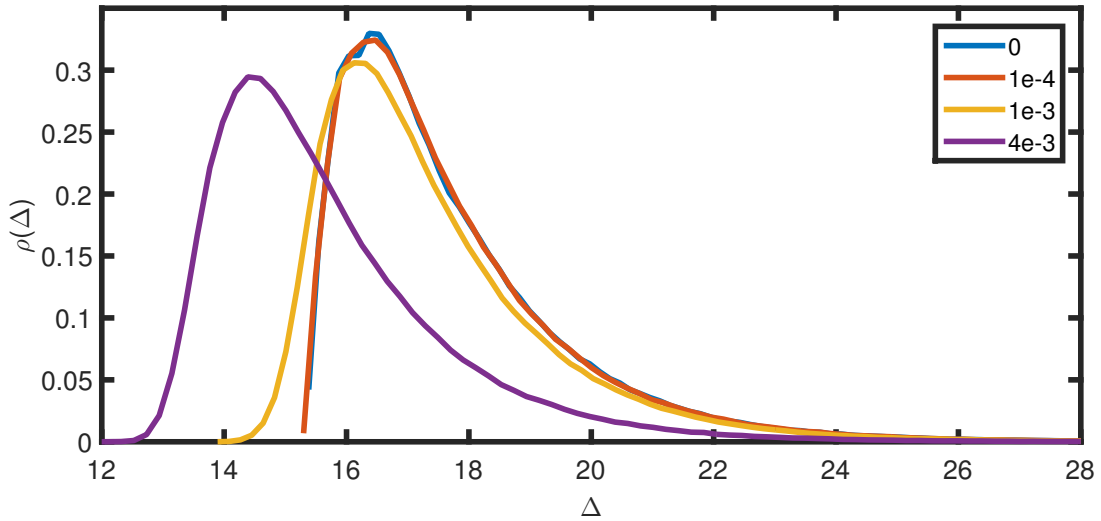
Figure 12: Probability density $\rho_\Delta(\Delta)$ of timings for the Shimizu–Morioka system calculated from the iterates derived map with noise strengths $\epsilon\sigma = 0$, 10^{-4}, 10^{-3} and 4×10^{-3} for parameters $\alpha = 0.4$ and $\lambda = 1.1954$.

where $\xi(t)$ is a white noise forcing, and σ is an $O(1)$ constant.

When $\sigma = 0$, this system has an unstable saddle at the origin, with a one-dimensional unstable direction and a two-dimensional unstable direction in which the dynamics are a focus. A sample trajectory for $\gamma = 0.7$ and $c = 1.108$ is shown in Figure 3 along with the nearby homoclinic orbit with $c \approx 1.107887$ which we label $H(t)$, and the time origin is such

that $H(t)$ takes its maxima at $t = 0$. We label the parameter values at which there exits a homoclinic orbit as $c = c_0(\gamma)$.

We again make the ansatz

$$x = \sum_k \theta_k H(t - t_k) + \epsilon R, \tag{162}$$

along with $c = c_0(\gamma) + \epsilon c_1$, for some sequence of widely separated times $\{t_k\}$ so that $H_k H_{k\pm 1} = O(\epsilon)$ and the polarity $\theta_k = \pm 1$ accounts for the symmetry $x \mapsto -x$.

The $O(\epsilon^0)$ equation is satisfied automatically, and the $O(\epsilon)$ equation is

$$\mathcal{L}_k R = c_1 \theta_k H_k - \frac{3}{\epsilon} H_k^2 (\theta_{k+1} H_{k+1} + \theta_{k-1} H_{k-1}) - \sigma \xi(t), \tag{163}$$

where

$$\mathcal{L}_k = \frac{\mathrm{d}^3}{\mathrm{d}t^3} + \gamma \frac{\mathrm{d}^2}{\mathrm{d}t^2} + \frac{\mathrm{d}}{\mathrm{d}t} - c_0 + 3H_k^2. \tag{164}$$

Now define the adjoint operator to $\mathcal{L}_k$,

$$\mathcal{L}_k^\dagger = -\frac{\mathrm{d}^3}{\mathrm{d}t^3} + \gamma \frac{\mathrm{d}^2}{\mathrm{d}t^2} - \frac{\mathrm{d}}{\mathrm{d}t} - c_0 + 3H_k^2, \tag{165}$$

and the null adjoint solution $N_k(t) \neq 0$ by

$$\mathcal{L}_k^\dagger N_k = 0. \tag{166}$$

Multiply the equation for R through by $N_k(t)$ and integrate to obtain

$$0 = c_1 \theta_k A - \frac{3}{\epsilon} \int_{-\infty}^\infty N_k H_k^2 (\theta_{k+1} H_{k+1} + \theta_{k-1} H_{k-1}) \, \mathrm{d}t - \sigma \int_{-\infty}^\infty N_k \xi \, \mathrm{d}t, \tag{167}$$

where

$$A = \int_{-\infty}^\infty c_1 N_k H_k \, \mathrm{d}t. \tag{168}$$

We know that

$$H \sim \begin{cases} h_0 e^{\lambda t} & \text{as } t \to -\infty, \\ h_\infty e^{-\mu t} \cos(\omega t + \phi) & \text{as } t \to \infty, \end{cases} \tag{169}$$

where λ is the unstable eigenvalue of the origin, and $-\mu \pm i\omega$ is the stable eigenvalue, for some h_0, h_∞ and ϕ.

Since the pulse train of homoclinic orbits are widely separated, we have that

$$3 \int_{-\infty}^\infty N_k H_k^2 H_{k+1} \, \mathrm{d}t \sim \int_{-\infty}^\infty N_k H_k^2 h_0 e^{\lambda(t - t_{k+1})} \, \mathrm{d}t \tag{170}$$

$$= 3h_0 e^{\lambda(t_k - t_{k+1})} \int_{-\infty}^\infty N_k H_k^2 e^{\lambda(t - t_k)} \, \mathrm{d}t \tag{171}$$

$$= 3h_0 e^{-\lambda(t_{k+1} - t_k)} \int_{-\infty}^\infty N H^2 e^{\lambda t} \, \mathrm{d}t \tag{172}$$

$$\equiv e^{-\lambda(t_{k+1} - t_k)} D \tag{173}$$

and also

$$3 \int_{-\infty}^{\infty} N_k H_k^2 H_{k-1} \ \mathrm{d}t \sim \int_{-\infty}^{\infty} N_k H_k^2 h_\infty e^{-\mu(t-t_{k-1})} \cos(\omega(t - t_{k-1}) + \phi) \ \mathrm{d}t \tag{174}$$

$$= 3h_\infty e^{-\mu(t_k - t_{k-1})} \left[\cos(\omega(t_k - t_{k-1}) + \phi) \int_{-\infty}^{\infty} NH^2 e^{-\mu t} \cos(\omega t) \ \mathrm{d}t \right.$$
$$\left. - \sin(\omega(t_k - t_{k-1}) + \phi) \int_{-\infty}^{\infty} NH^2 e^{-\mu t} \sin(\omega t) \ \mathrm{d}t \right] \tag{175}$$

$$\equiv e^{-\mu(t_k - t_{k-1})} \cos(\omega(t_k - t_{k-1}) + \Phi) B \tag{176}$$

Defining the time interval between pulses $\Delta_k \equiv t_k - t_{k-1}$, we obtain

$$\theta_{k+1} e^{-\lambda \Delta_{k+1}} = \epsilon \theta_k C + \theta_{k-1} E e^{-\mu \Delta_k} \cos(\omega \Delta_k + \Phi) + \epsilon \sigma M \eta_k, \tag{177}$$

where $\eta_k \sim \mathcal{N}(0, 1)$, and

$$C = \frac{A}{D}, \tag{178}$$

$$E = -\frac{B}{D}, \tag{179}$$

$$M^2 = \left(\frac{1}{D} \right)^2 \int_{-\infty}^{\infty} N^2 \ \mathrm{d}t. \tag{180}$$
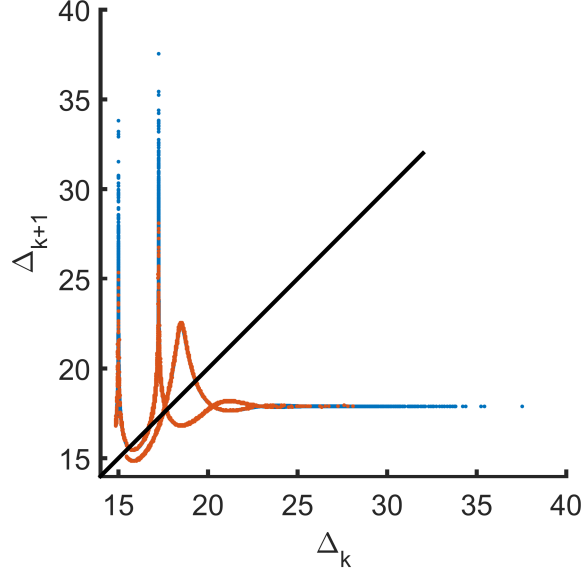
Figure 13: Times between pulses for the deterministic timing map (177) iterated 10^6 times (blue) and a full numerical simulation with 5500 pulses (red) for $c = 1.108$ and $\gamma = 0.7$.

To verify that we have obtained the correct timing map, we first remove the noise term, setting $\sigma = 0$. Figure 13 shows a comparison of the times between pulses for a full numerical
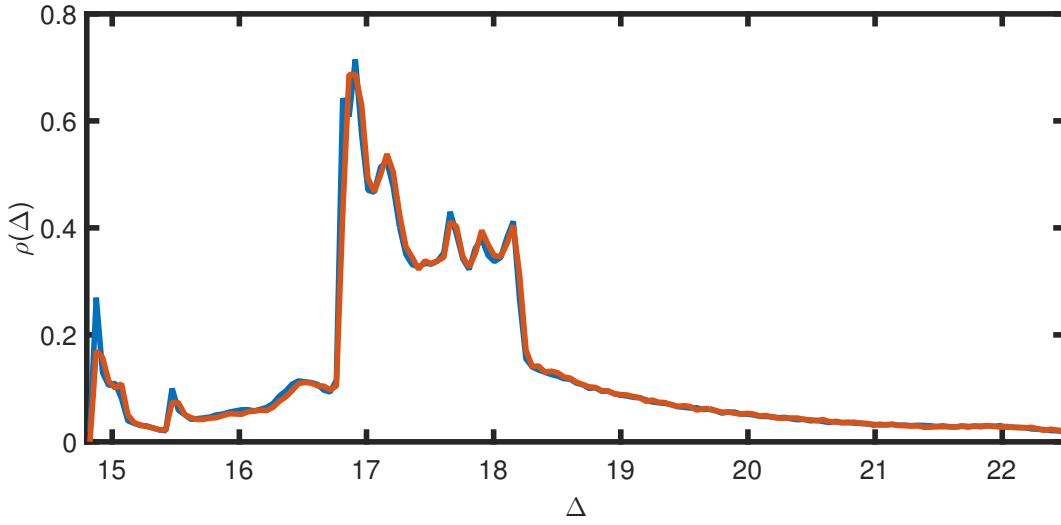
Figure 14: Probability density of times between pulses for the timing map (177) iterated 10^6 times (blue) and a full numerical simulation with 560 000 pulses (red) for $c = 1.108$ and $\gamma = 0.7$ with noise strength $\epsilon\sigma = 10^{-6}$.
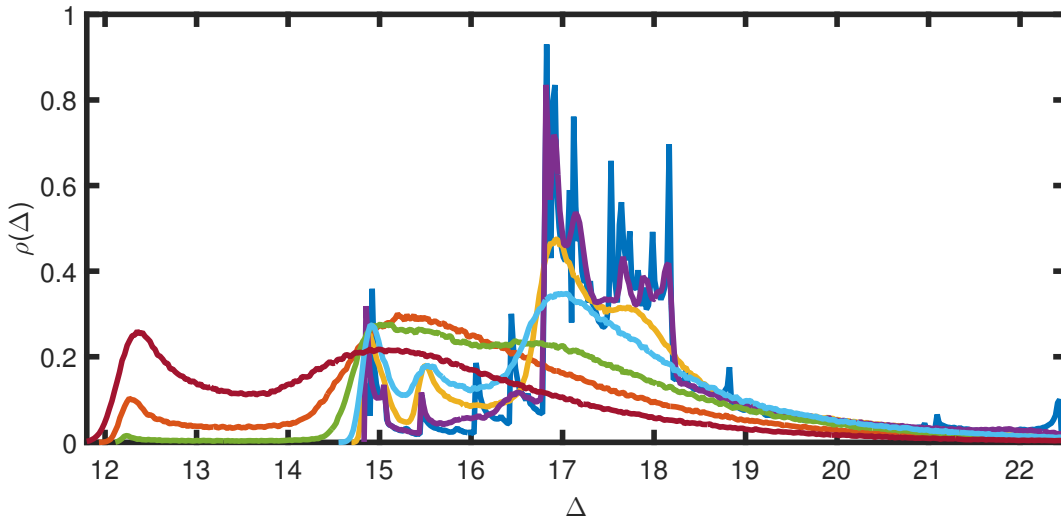
Figure 15: The pdf for the timing map (177) for noise strengths $\epsilon\sigma = 0$ (dark blue), 10^{-6} (purple), 10^{-5} (orange), 2×10^{-5} (light blue), 5×10^{-5} (green), 10^{-4} (red) and 2×10^{-4} (magenta).

simulation of (161) and the derived timing map (177) iterated 10^6 times for $c = 1.108$ and $\gamma = 0.7$. The agreement is excellent.

Figure 14 shows a comparison of the probability density of timings $\rho(\Delta)$ for noise strength $\epsilon\sigma = 10^{-6}$ for the timing map (177) iterated 10^6 times and a direct numerical

computation of (161) for 560 000 pulses. The agreement is excellent, and so we now deal only with the map.

Figure 15 shows the probability density of timings $\rho(\Delta)$ for a range of noise strengths, as well as the deterministic invariant measure normalised to be a probability density. For very small noise strengths, the peaks of the invariant measure are simply rounded off. For larger noise strengths, the peaks in the invariant measure are fully homogenised, and a new smooth peak begins to arise at smaller Δ. Appendix B shows images of the stationary distribution for a large range of ϵc_1 and $\epsilon \sigma$. The main features are that as noise strength is increased, it affects large Δ and small c_1 first. We see clearly that attractors with high Δ are rapidly smoothed out, and the densities begin to be centered around attractors at lower Δ. There is also evidence of exponential tails at large Δ. This is to be expected, since

$$\rho_\Delta(\Delta) = \lambda e^{-\lambda \Delta} \rho_z(e^{-\lambda \Delta}) \sim \lambda e^{-\lambda \Delta} \rho_z(0) \quad \text{as } \Delta \to \infty, \tag{181}$$

and so we obtain exponential tails provided that $\rho_z(0)$ is bounded. We can demonstrate this by observing that

$$\rho_z(0) = \frac{1}{\sqrt{2\pi a^2}} \int e^{-[f(s)]^2/2a^2} \rho_z(s) \, \mathrm{d}s \leq \frac{1}{\sqrt{2\pi a^2}} \int \rho_z(s) \, \mathrm{d}s = \frac{1}{\sqrt{2\pi a^2}}. \tag{182}$$
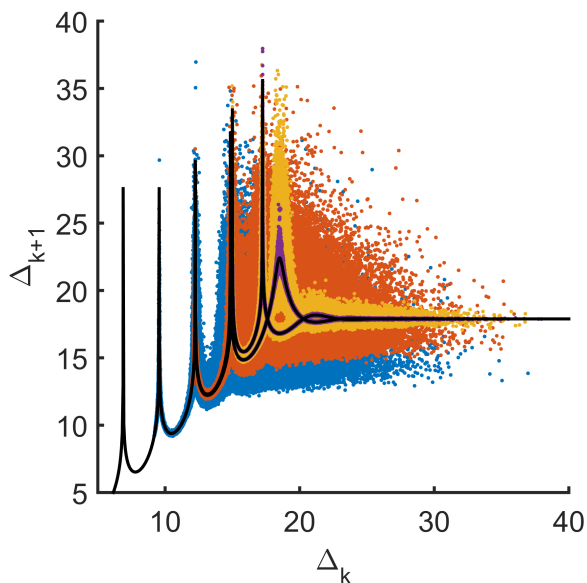
Figure 16: Times between pulses for the timing map (177) iterated 10^6 times for noise strength $\epsilon \sigma = 10^{-6}$ (purple), 10^{-5} (yellow), 10^{-4} (red) and 4×10^{-4} (blue) and the deterministic timing map (177) (black lines).

To investigate the emergence of the new peak in the probability density $\rho(\Delta)$, in Figure 16 we plot iterates of the timing map (177) for various noise strengths $\epsilon \sigma$ along with the full deterministic map. For the deterministic case, iterates of this map reside in the attracting set which has $\Delta \gtrsim 15$, see Figure 13. For very weak noise, the attracting set remains much

the same, but is simply smoothed out a little. Larger noise strengths blur the deterministic attracting set completely, but in addition begin to realise, and are attracted to, parts of the deterministic map at smaller Δ. Such phenomena have been observed by numerous authors, and are often referred to as 'noise induced boundary crises' [11, 8].

There is also a noise threshold beyond which a significant number of trajectories are attracted to the peak in the deterministic map just to the left of $\Delta = 10$ beyond which the map breaks down, and iterates diverge to $-\infty$. This can be rationalised by noticing that the time of flight for $H(t)$ is approximately 10, and so $\Delta < 10$ represents solutions that do not visit the origin at all, and the assumption of widely spaced pulses is no longer valid.

5   Conclusions

Through generalising the singular perturbation analysis of homoclinic pulse dynamics in ODEs [4] to stochastic systems, we have demonstrated that for a large class of near-homoclinic dynamical systems, the most significant effect of noise on the timing between homoclinic pulses and on the position of return of trajectories to the origin is due to a cumulative effect of noise on the trajectory away from the origin, rather than the details of the dynamics near to the origin as originally conjectured by Stone and Holmes [17]. This cumulative effect may be interpreted as providing a random kick sampled from a well-defined normal distribution to a deterministic trajectory just as it enters any domain of interest centred around and close to the origin, and that this kick is asymptotically large when compared to the effect of noise within this domain, in which its role is simply to provide a buffer region of size $O(\epsilon)$ about the stable manifold from which the stochastic trajectory is ejected, preventing trajectories from remaining within the domain.

We are able to make good analytical progress in the two-dimensional Duffing system since the resulting return map has a stable fixed point that we can expand around. For sufficiently small amplitude noise, the dynamics are controlled by the distance from homoclinicity, whilst for sufficiently large amplitude noise, the dynamics is controlled by the noise by creating an effective distance from homoclinicity based on the standard deviation of the resulting stationary distribution of the return map.

The derived maps for the Shimizu–Morioka model have nearly the same functional form as the Duffing system, but the parameter values here allow chaotic solutions. In this system we demonstrated that the singular perturbation analysis is easily generalisable to inherently multidimensional dynamics.

The derived maps for Shilnikov system have a rich and varied behaviour, as shown in Appendix B. Noise acts to smooth out the deterministic system, first at small deviations from homoclinicity and large spacings, and eventually at all parameter values as the noise amplitude is increased from zero. We also see noise induced boundary crises [11, 8] in which the presence of noise causes the stationary distribution to no longer be centered around the large spacing deterministic attractor, but to swap to another deterministic attractor at smaller spacing.

In all systems we observe exponential tails in the distribution of timing spacings as in Stone and Holmes [18], but note that this phenomenon is simply a manifestation of a change of variables from return points to timings.

We have developed a toolbox for investigating the effects of noise on homoclinic trajectories and have applied it to the two canonical homoclinic bifurcation scenarios, Lorenz and Shilnikov. Looking forward, we are now in a position to investigate more exotic systems like heteroclinic networks, bifocal orbits and excitable systems.

We also wish to apply the ideas contained withing this report to PDEs that contain traveling wave solutions that are of homoclinic or heteroclinic type. Near-homoclinic pulses can be interpreted as coherent structures in a number of physically relevant PDEs with traveling wave solutions [3]. A canonical example would be the real Ginzburg–Landau equation which has 'kink' solutions that connect two equilibria. It is know that an initial distribution of kinks that connect back and forth between the two equilibria will evolve in time to collide and annihilate each other in finite exponential time [3]. Given the results presented here, it seems likely that for stochastic dynamics, these annihilations will still occur, but instead because the kinks will begin to behave like Brownian random walkers.

References

[1] D. ARMBRUSTER, E. STONE, AND V. KIRK, *Noisy heteroclinic networks*, Chaos: An Interdisciplinary Journal of Nonlinear Science, 13 (2003), p. 71.

[2] A. ARNEODO, P. H. COULLET, AND E. A. SPIEGEL, *The dynamics of triple convection*, vol. 31, 1985.

[3] N. BALMFORTH, *Solitary Waves and Homoclinic Orbits*, Annual Review of Fluid Mechanics, 27 (1995), pp. 335–374.

[4] N. J. BALMFORTH, G. R. IERLEY, AND E. A. SPIEGEL, *Chaotic Pulse Trains*, SIAM Journal on Applied Mathematics, 54 (1994), pp. 1291–1334.

[5] M. EGUIA AND G. MINDLIN, *Distribution of interspike times in noise-driven excitable systems*, Physical Review E, 61 (2000), pp. 6490–6499.

[6] C. W. GARDINER, *Handbook of stochastic methods*, Springer, 1985.

[7] P. GLENDINNING AND C. SPARROW, *Local and global behavior near homoclinic orbits*, Journal of Statistical Physics, 35 (1984), pp. 645–696.

[8] R. E. LEE DEVILLE, E. VANDEN-EIJNDEN, AND C. B. MURATOV, *Two distinct mechanisms of coherence in randomly perturbed dynamical systems*, Physical Review E - Statistical, Nonlinear, and Soft Matter Physics, 72 (2005), pp. 1–10.

[9] B. T. NADIGA AND B. P. LUCE, *Global Bifurcation of Shilnikov Type in a Double-Gyre Ocean Model*, Journal of Physical Oceanography, 31 (2001), pp. 2669–2690.

[10] R. P. AND P. TALKNER, *Invariant densities for noisy maps*, Physical Review A, 44 (1991), pp. 6348–6363.

[11] A. PIKOVSKY AND J. KURTHS, *Coherence Resonance in a Noise-Driven Excitable System*, Physical Review Letters, 78 (1997), pp. 775–778.

[12] A. L. SHIL'NIKOV, *On bifurcations of the Lorenz attractor in the Shimizu-Morioka model*, Physica D: Nonlinear Phenomena, 62 (1993), pp. 338–346.

[13] L. P. SHILNIKOV, *A Contribution To the Problem of the Structure of an Extended Neighborhood of a Rough Equilibrium State of Saddle-Focus Type*, Mathematics of the USSR-Sbornik, 10 (1970), pp. 91–102.

[14] T. SHIMIZU AND N. MORIOKA, *On the bifurcation of a symmetric limit cycle to an asymmetric one in a simple model*, Physics Letters, 76 (1980), pp. 201–204.

[15] E. SIMONNET, M. GHIL, AND H. DIJKSTRA, *Homoclinic bifurcations in the quasi-geostrophic double-gyre circulation*, Journal of Marine Research, 63 (2005), pp. 931–956.

[16] E. STONE AND D. ARMBRUSTER, *Noise and O(1) amplitude effects on heteroclinic cycles.*, Chaos (Woodbury, N.Y.), 9 (1999), pp. 499–506.

[17] E. STONE AND P. HOLMES, *Random Perturbations of Heteroclinic Attractors*, SIAM Journal on Applied Mathematics, 50 (1990), pp. 726–743.

[18] ——, *Unstable fixed points, heteroclinic cycles and exponential tails in turbulence production*, Physics Letters A, 155 (1991), pp. 29–42.

A   Separating the directions of noise near the Duffing saddle

A.1   Noisy stable direction, $\xi_{x_1} \neq 0$ in $\mathcal{D}$

In this case, the deterministic results for x_2 still hold, and so the nth residence time t_n still satisfies

$$t_n = \frac{1}{\lambda} \log\left(\frac{\delta}{z_n}\right), \tag{183}$$

provided that z_n is known. Since we know that upon entrance we have $x_1 = \delta$, we wish to solve the Ornstein-Uhlenbeck process for x_1 for the transition probability density

$$\rho(x_1, t_n | \delta, 0). \tag{184}$$

The known solution to for x_1 is

$$\rho(x_1, t_n | \delta, 0) = \mathcal{N}_{x_1}\left(\delta e^{-\mu t_n}, \frac{\epsilon^2}{2\mu}(1 - e^{-2\mu t_n})\right) \tag{185}$$

$$= \mathcal{N}_{x_1}\left(\delta^{1-\mu/\lambda} z_n^{\mu/\lambda}, \frac{\epsilon^2}{2\mu}(1 - \delta^{-2\mu/\lambda} z_n^{2\mu/\lambda})\right) \tag{186}$$

This transition probability density is the the probability density of the exit points w_n.

Recalling the linear mapping

$$z_{n+1} = \alpha w_n + c, \tag{187}$$

along with standard results for linear combinations of normally distributed random variables, we see that

$$\rho(z_{n+1} | z_n) = \mathcal{N}_z\left(\alpha \delta^{1-\mu/\lambda} z_n^{\mu/\lambda} + c, \frac{\alpha^2 \epsilon^2}{2\mu}(1 - \delta^{-2\mu/\lambda} z_n^{2\mu/\lambda})\right). \tag{188}$$

Finally, since $t_n = -\log(z_n/\delta)/\lambda$, we have

$$\rho(t_{n+1} | t_n) \approx \begin{cases} \lambda e^{-\lambda t} \mathcal{N}_{e^{-\lambda t}}\left(\alpha e^{-\mu t_n} + c/\delta, \frac{\alpha^2 \epsilon^2}{2\mu \delta^2}(1 - e^{-2\mu t_n})\right) & \text{for } \delta \gg c \gg \epsilon, \\ 2\lambda e^{-\lambda t} \mathcal{N}_{e^{-\lambda t}}\left(\alpha e^{-\mu t_n}, \frac{\alpha^2 \epsilon^2}{2\mu \delta^2}(1 - e^{-2\mu t_n})\right) & \text{for } c \ll \epsilon. \end{cases} \tag{189}$$

For long residency times with $\mu t_n \gg 1$, which is valid for δ small enough such that the deterministic trajectories are very close to the homoclinic orbit, we can make the approximation $e^{-\mu t_n} \approx 0$. This is formally equivalent to assuming that trajectories through $\mathcal{D}$ attain a statistically steady state before leaving $\mathcal{D}$. In this case, we obtain

$$\rho^s(w_n) = \mathcal{N}_w\left(0, \frac{\epsilon^2}{2\mu}\right), \tag{190}$$

$$\rho^s(z_n) = \mathcal{N}_z\left(c, \frac{\alpha^2 \epsilon^2}{2\mu}\right), \tag{191}$$

$$\rho^s(t_n) = \begin{cases} \lambda e^{-\lambda t} \mathcal{N}_{e^{-\lambda t}}\left(\frac{c}{\delta}, \frac{\alpha^2 \epsilon^2}{2\mu \delta^2}\right) & \text{for } \delta \gg c \gg \epsilon, \\ 2\lambda e^{-\lambda t} \mathcal{N}_{e^{-\lambda t}}\left(0, \frac{\alpha^2 \epsilon^2}{2\mu \delta^2}\right) & \text{for } c \ll \epsilon. \end{cases} \tag{192}$$

In particular, $\mathbb{E}^s(w_n)$ and $\mathbb{E}^s(z_n)$ are the same as the deterministic result either under the assumption that $\mu t_n \gg 1$ or in the limit $n \to \infty$.

Also, for $\epsilon \ll c \ll \delta \ll 1$ we have

$$\mathbb{E}^s(t_n) = \int_0^\infty \frac{\lambda t e^{-\lambda t}}{\sqrt{\pi \alpha^2 \epsilon^2 / \mu \delta^2}} \exp\left[-\frac{(e^{-\lambda t} - c/\delta)^2}{\alpha^2 \epsilon^2 / \mu \delta^2}\right] dt \tag{193}$$

$$\sim \frac{1}{\sqrt{\pi \alpha^2 \epsilon^2 / \mu \delta^2}} \int_{-\infty}^\infty \lambda t_* e^{-\lambda t_*} e^{-\lambda^2 c^2 \mu (t - t_*)^2 / \alpha^2 \epsilon^2} dt \tag{194}$$

$$\sim \frac{\alpha \epsilon \sqrt{\pi} t_* e^{-\lambda t_*}}{c \sqrt{\mu \pi \alpha^2 \epsilon^2 / \mu \delta^2}} \tag{195}$$

$$\sim \frac{1}{\lambda} \log\left(\frac{\delta}{c}\right), \tag{196}$$

which matches the deterministic result for $c \neq 0$, where $t_* = \log(\delta/c)/\lambda$ is the stationary point of the term in the second exponential, and we have employed Laplace's method for approximating integrals, with large parameter δ^2 / ϵ^2.

For $c \ll \epsilon$ we have

$$\mathbb{E}^s(t_n) = \int_0^\infty \frac{2\lambda t e^{-\lambda t}}{\sqrt{\pi \alpha^2 \epsilon^2 / \mu \delta^2}} \exp\left[-\frac{e^{-2\lambda t}}{\alpha^2 \epsilon^2 / \mu \delta^2}\right] dt \tag{197}$$

$$= \int_0^1 \frac{2}{\lambda \sqrt{\pi \alpha^2 \epsilon^2 / \mu \delta^2}} \log\left(\frac{1}{y}\right) \exp\left[-\frac{y^2}{\alpha^2 \epsilon^2 / \mu \delta^2}\right] dy \tag{198}$$

$$= \int_0^{\delta\sqrt{\mu}/\alpha\epsilon} \frac{2}{\lambda \sqrt{\pi}} \log\left(\frac{\delta\sqrt{\mu}}{\alpha \epsilon s}\right) e^{-s^2} ds \tag{199}$$

$$\sim \int_0^\infty \frac{2}{\lambda \sqrt{\pi}} \log\left(\frac{\delta\sqrt{\mu}}{\alpha \epsilon s}\right) e^{-s^2} ds \tag{200}$$

$$= \int_0^\infty \frac{2}{\lambda \sqrt{\pi}} \log\left(\frac{\delta}{\epsilon}\right) e^{-s^2} ds + \int_0^\infty \frac{2}{\lambda \sqrt{\pi}} \log\left(\frac{\sqrt{\mu}}{\alpha s}\right) e^{-s^2} ds \tag{201}$$

$$\sim \frac{1}{\lambda} \log\left(\frac{\delta}{\epsilon}\right), \tag{202}$$

since the second integral in (201) is just some $O(1)$ number. This is the same result as for noise uniformly every within $\mathcal{D}$.

Figure 17 shows a comparison between a direct numerical simulation for the return and leave probability densities $\rho(z_n)$ and $\rho(w_n)$ respectively, and their long residency time asymptotic stationary limit for $\gamma = 0.08$, $\beta = 0.01$, $\delta = 0.1$, $\epsilon = 0.0006$, $\alpha = 1$ and $c = 0$. There is clearly a very good match. The mean of $t_n = \log(\delta/|z_n|)/\lambda$ is 6.264, and the value of its asymptotic result $\log(\delta/\epsilon)/\lambda$ is 5.325.

A.2   Noisy unstable direction, $\xi_{x_2} \neq 0$ in $\mathcal{D}$

In this case we have $x_1 = \delta e^{-\mu t}$ and x_2 satisfies the unstable Ornstein-Uhlenbeck process with transition density

$$\rho(x_2, t | z_n, 0) = \mathcal{N}_{x_2}\left(z_n e^{\lambda t}, \frac{\epsilon^2}{2\lambda}(e^{2\lambda t} - 1)\right) \tag{203}$$
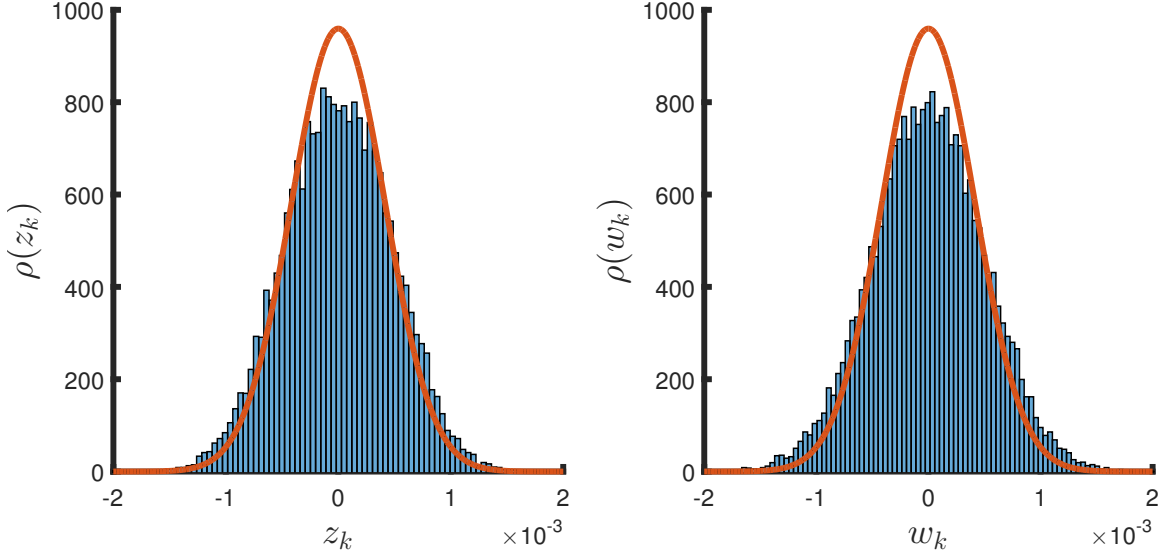
Figure 17: Left: Probability density of return points z_k to $\mathcal{D}$ with $\delta = 0.1$ and noise strength $\epsilon = 0.0006$ acting only in the stable direction of the saddle, for parameters $\gamma = 0.08$ and $\beta = 0.1$ for a direct numerical simulation with 2250 returns to $\mathcal{D}$ (blue histogram) and the long residency time asymptotic stationary distribution (191) with $\alpha = 1$ and $c = 0$ (red line). Right: Leave points w_k.

In the case of large times, $\lambda t \gg 1$ we get

$$\rho(x_2, t | z_n, 0) \sim \mathcal{N}\left(z_n e^{\lambda t}, \frac{\epsilon^2}{2\lambda} e^{2\lambda t}\right) \tag{204}$$

In this limit we also have $w_n \approx 0$, and so $z_{n+1} \sim c$ provided that c is not too small.

In order to find the exit point w_n we need a distribution for the time taken for x_2 to leave $\mathcal{D}$. We have by definition

$$\mathbb{P}(t_n > t) = \int_{-\delta}^{\delta} \rho(x_2, t | z_n, 0) \, \mathrm{d}x_2 \tag{205}$$

$$= \int_{-\delta}^{\delta} \sqrt{\frac{\lambda}{\pi \epsilon^2 (e^{2\lambda t} - 1)}} \exp\left[-\frac{\lambda (z - z_n e^{\lambda t})^2}{\epsilon^2 (e^{2\lambda t} - 1)}\right] \mathrm{d}z \tag{206}$$

$$= \frac{1}{2}\left[\mathrm{erf}\left(\frac{\delta - z_n e^{\lambda t}}{\sigma(t)}\right) + \mathrm{erf}\left(\frac{\delta + z_n e^{\lambda t}}{\sigma(t)}\right)\right], \tag{207}$$

where $\sigma(t)^2 = \epsilon^2(e^{2\lambda t} - 1)/\lambda \sim \epsilon^2 e^{2\lambda t}/\lambda$. Note that under the assumption that $z_n \sim c$, the error functions have widely different expansions in all the cases $c \ll \epsilon \ll \delta$, $\epsilon \ll c \ll \delta$, $\epsilon \gg \delta e^{-\lambda t}$ and $c \gg \delta e^{-\lambda t}$, due to the exponential expansion casing rapid reordering of terms.

Define $b_\pm(t) = (\delta \pm z_n e^{\lambda t})/\sigma(t)$. Then,

$$\rho(t_n|z_n) = \frac{\mathrm{d}}{\mathrm{d}t}\left(1 - \mathbb{P}(t_n > t)\right) \tag{208}$$

$$= -\frac{1}{\sqrt{\pi}}\left[b'_+ e^{-b_+^2} + b'_- e^{-b_-^2}\right] \tag{209}$$

$$= \sqrt{\frac{\lambda^3}{\pi\epsilon^2(e^{2\lambda t}-1)^3}}\left[(\delta e^{2\lambda t} + z_n e^{\lambda t})\exp\left(-\frac{\lambda(\delta + z_n e^{\lambda t})^2}{\epsilon^2(e^{2\lambda t}-1)}\right)\right.$$
$$\left. + (\delta e^{2\lambda t} - z_n e^{\lambda t})\exp\left(-\frac{\lambda(\delta - z_n e^{\lambda t})^2}{\epsilon^2(e^{2\lambda t}-1)}\right)\right] \tag{210}$$

$$= \sqrt{\frac{\lambda^3}{\pi\epsilon^2(1-e^{-2\lambda t})^3}}\left[(\delta e^{-\lambda t} + z_n e^{-2\lambda t})\exp\left(-\frac{\lambda(\delta e^{-\lambda t} + z_n)^2}{\epsilon^2(1-e^{-2\lambda t})}\right)\right.$$
$$\left. + (\delta e^{-\lambda t} - z_n e^{-2\lambda t})\exp\left(-\frac{\lambda(\delta e^{-\lambda t} - z_n)^2}{\epsilon^2(1-e^{-2\lambda t})}\right)\right] \tag{211}$$

Then, since $w_n = \delta e^{-\mu t_n}$, we have

$$\rho(w_n|z_n) = \frac{1}{2\mu w_n}\sqrt{\frac{\lambda^3}{\pi\epsilon^2(1-(w_n/\delta)^{2\lambda/\mu})^3}}$$
$$\left[(\delta(w_n/\delta)^{\lambda/\mu} + z_n(w_n/\delta)^{2\lambda/\mu})\exp\left(-\frac{\lambda(\delta(w_n/\delta)^{\lambda/\mu} + z_n)^2}{\epsilon^2(1-(w_n/\delta)^{2\lambda/\mu})}\right)\right.$$
$$\left. + (\delta(w_n/\delta)^{\lambda/\mu} - z_n(w_n/\delta)^{2\lambda/\mu})\exp\left(-\frac{\lambda(\delta(w_n/\delta)^{\lambda/\mu} - z_n)^2}{\epsilon^2(1-(w_n/\delta)^{2\lambda/\mu})}\right)\right]. \tag{212}$$

Finally, since $z_{n+1} = \alpha w_n + c$, we obtain the transtion density

$$\rho(z_{n+1}|z_n) = \frac{1}{2\mu(z_{n+1}-c)}\sqrt{\frac{\lambda^3}{\pi\epsilon^2(1-((z_{n+1}-c)/\alpha\delta)^{2\lambda/\mu})^3}}$$
$$\left[(\delta((z_{n+1}-c)/\alpha\delta)^{\lambda/\mu} + z_n((z_{n+1}-c)/\alpha\delta)^{2\lambda/\mu})\right.$$
$$\exp\left(-\frac{\lambda(\delta((z_{n+1}-c)/\alpha\delta)^{\lambda/\mu} + z_n)^2}{\epsilon^2(1-((z_{n+1}-c)/\alpha\delta)^{2\lambda/\mu})}\right)$$
$$+ (\delta((z_{n+1}-c)/\alpha\delta)^{\lambda/\mu} - z_n(z_{n+1}-c)/\alpha\delta)^{2\lambda/\mu})$$
$$\left.\exp\left(-\frac{\lambda(\delta((z_{n+1}-c)/\alpha\delta)^{\lambda/\mu} - z_n)^2}{\epsilon^2(1-((z_{n+1}-c)/\alpha\delta)^{2\lambda/\mu})}\right)\right]. \tag{213}$$

Note that unless $\lambda/\mu = 1$, these distributions are not Gaussian, since for example, $\rho(w_n = 0|z_n) = \infty$. In general, we have $\lambda/\mu = 1 - \epsilon\gamma + O(\epsilon^2)$.

We can approximately find stationary distriubtions by the relation

$$\rho^s(z) = \int_{-\infty}^{\infty}\rho(z|s)\rho^s(s)\,\mathrm{d}s = \lim_{n\to\infty}\frac{1}{n}\sum_{i=1}^{n}\rho(z|z_i), \tag{214}$$

where z_i is some predetermined sequence of known values of the stochastic process. For this, we can use DNS of the equations of motion to produce a sequence $\{z_i\}_1^n$ for some large n, and estimate ρ^s.
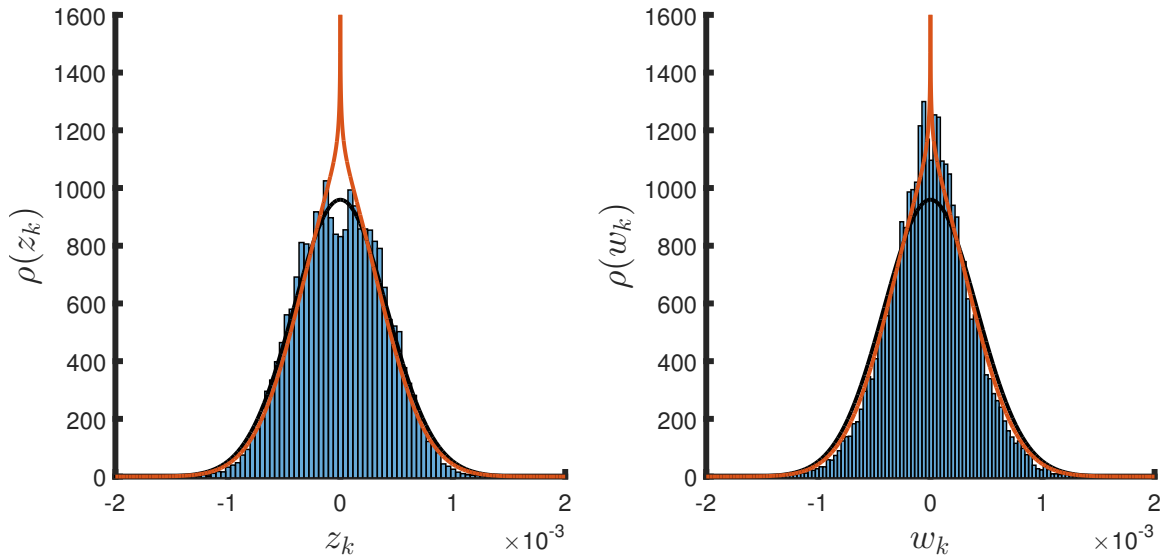

Figure 18: Probability density of return points z_k to $\mathcal{D}$ with $\delta = 0.1$ and noise strength $\epsilon = 0.0006$ acting only in the unstable direction of the saddle, for parameters $\gamma = 0.08$ and $\beta = 0.1$ for a direct numerical simulation with 2250 returns to $\mathcal{D}$ (blue histogram) and the long residency time asymptotic stationary distribution approximation (214) with $\alpha = 1$ and $c = 0$ (red line). Right: leave points w_k.

Figure 18 shows a comparison between a direct numerical simulation for the return and leave probability densities $\rho(z_n)$ and $\rho(w_n)$ respectively, and their stationary approximations using (214) for $\gamma = 0.08$, $\beta = 0.01$, $\delta = 0.1$, $\epsilon = 0.0006$, $\alpha = 1$ and $c = 0$. Plotted also is the Gaussian distribution for noise in the *stable* direction only. The leaving distribution $\rho(w_n)$ is well approximated by the result here, and is clearly non-Gaussian. The return distribution $\rho(z_n)$ is more closely Gaussian, and suggests that the linear approximation $z_{n+1} = \alpha z_n + c$ is not completely valid.

B Stationary probability densities $\rho_\Delta(\Delta)$ for the Shilnikov system
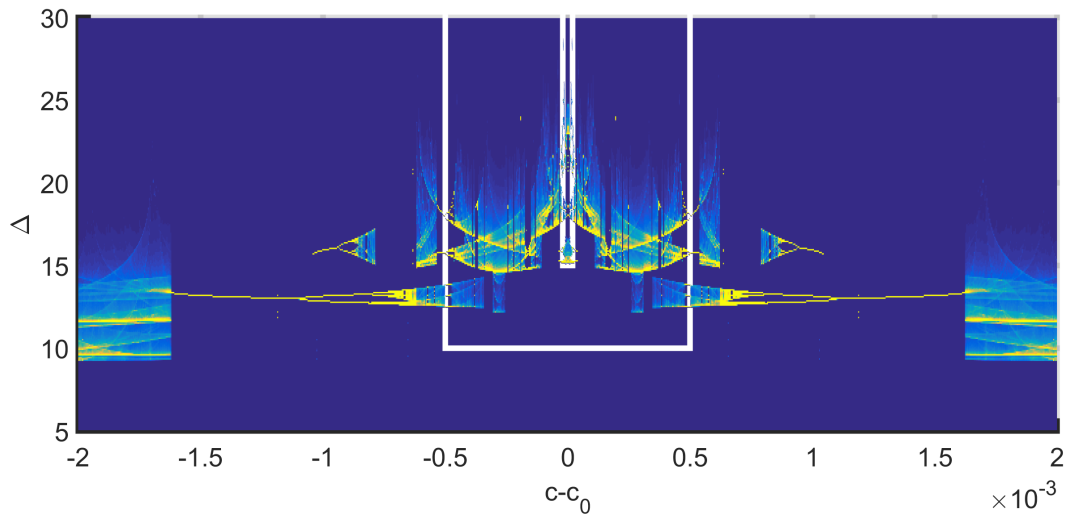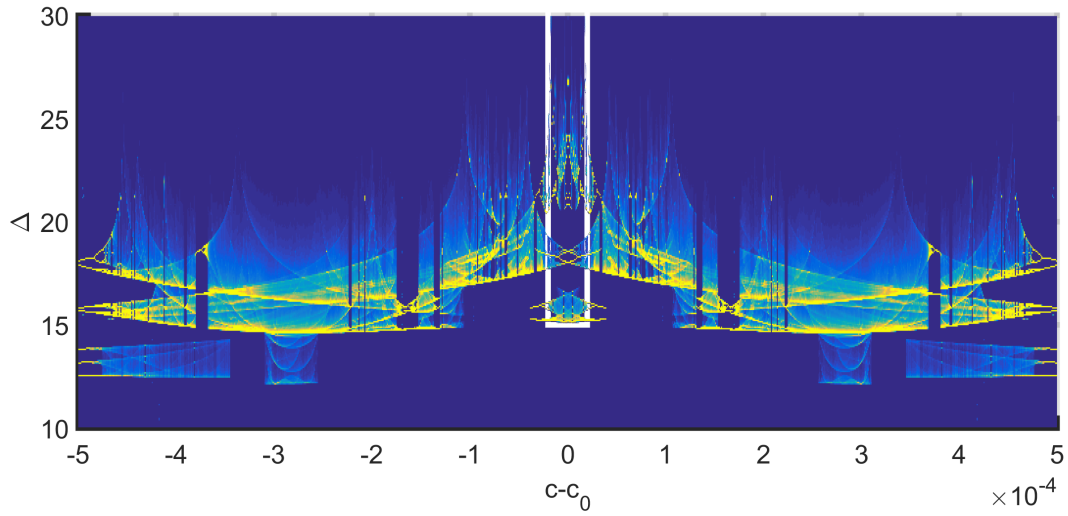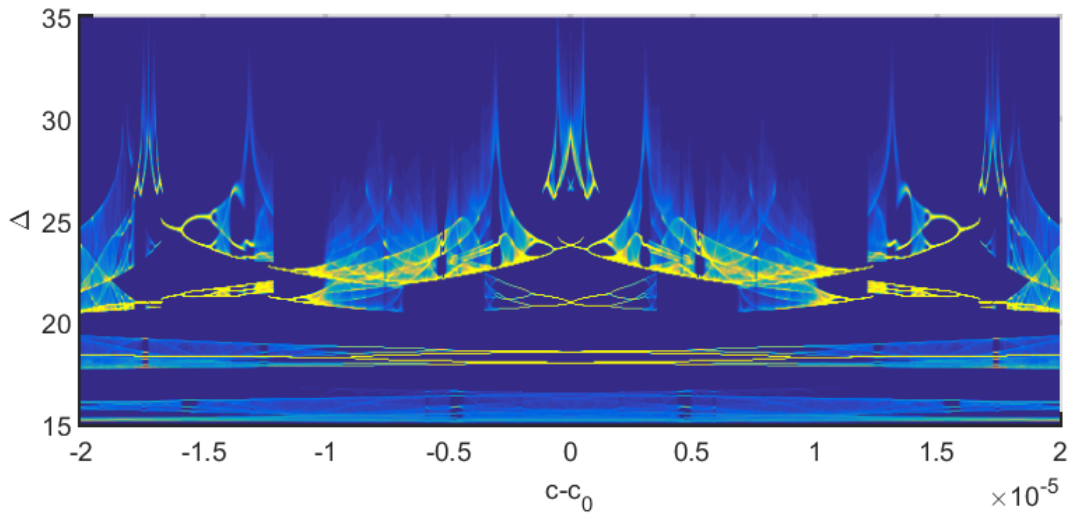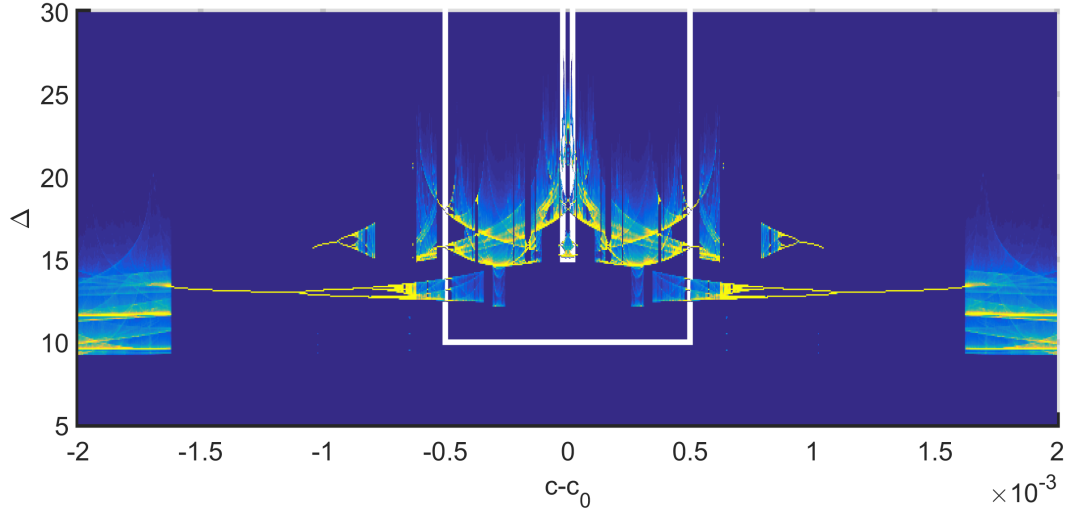
B.1 $\epsilon\sigma = 0$
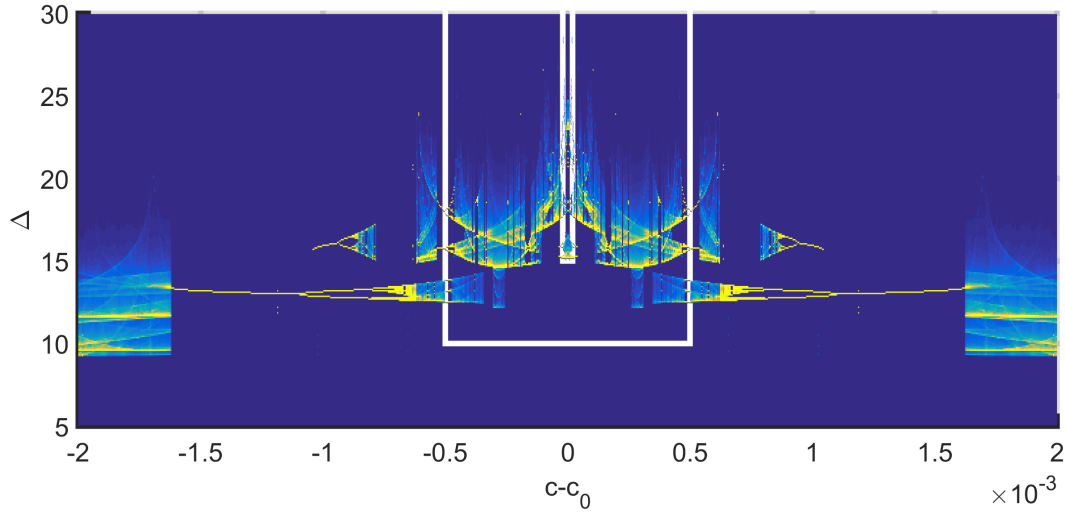
Figure 19: Stationary probability density $\rho_\Delta(\Delta)$ of the timing map (177) for the Shilnikov system for noise strength $\epsilon\sigma = 0$. Color from blue to yellow represents low to high values. Scale is arbitrary. White lines show regions plotted in Figures 20 and 21.
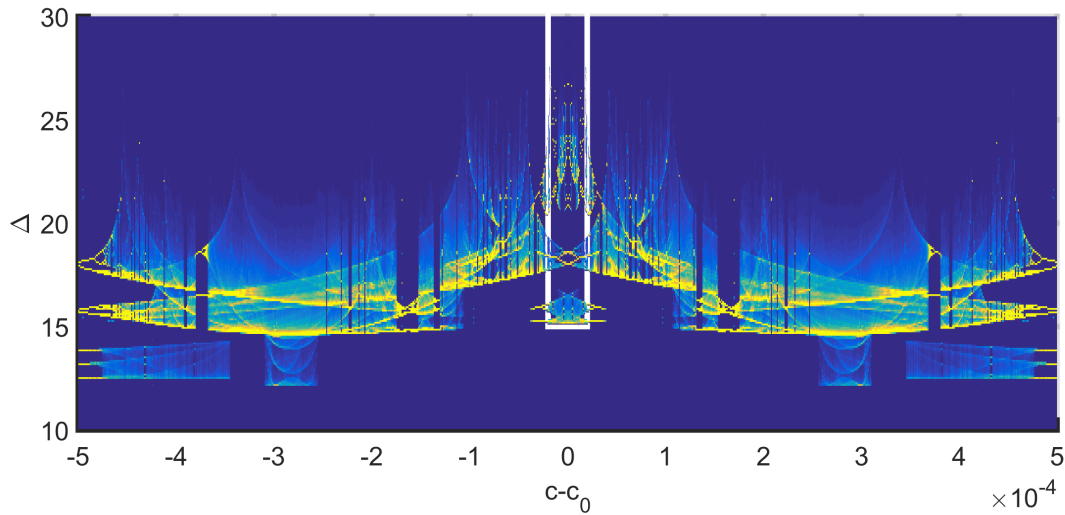
Figure 20: Stationary probability density $\rho_\Delta(\Delta)$ of the timing map (177) for the Shilnikov system for noise strength $\epsilon\sigma = 0$. Color from blue to yellow represents low to high values. Scale is arbitrary. White lines show region plotted in Figure 21.
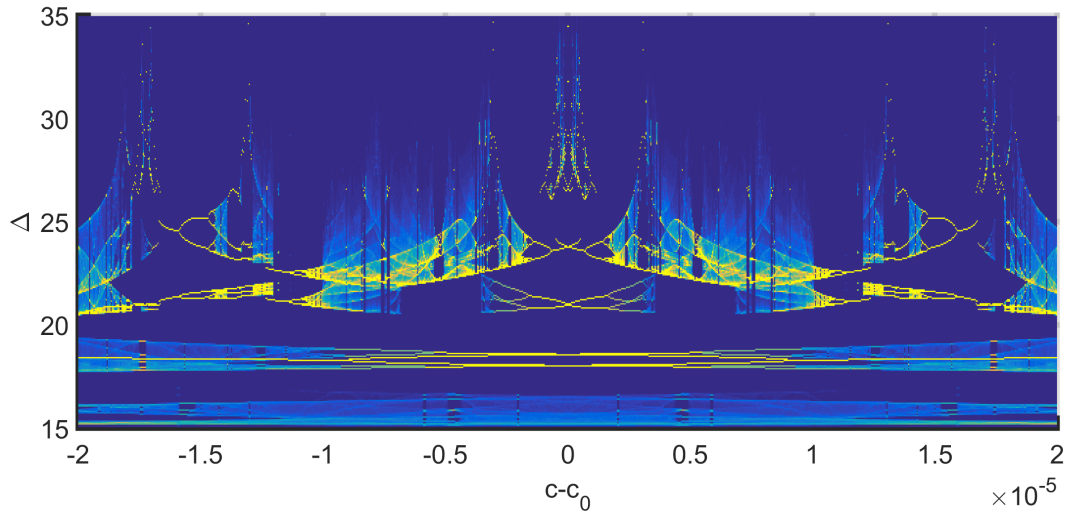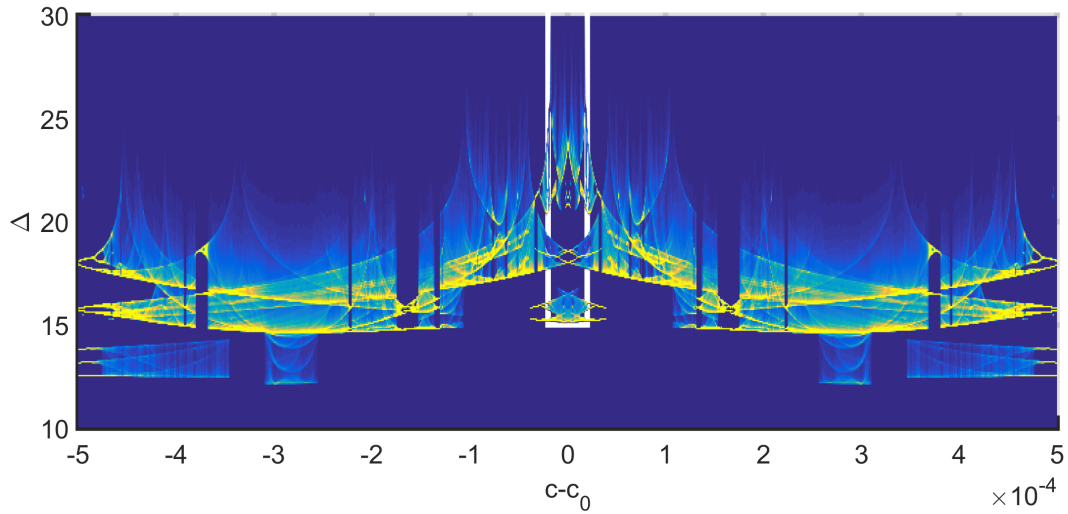
Figure 21: Stationary probability density $\rho_\Delta(\Delta)$ of the timing map (177) for the Shilnikov system for noise strength $\epsilon\sigma = 0$. Color from blue to yellow represents low to high values. Scale is arbitrary.
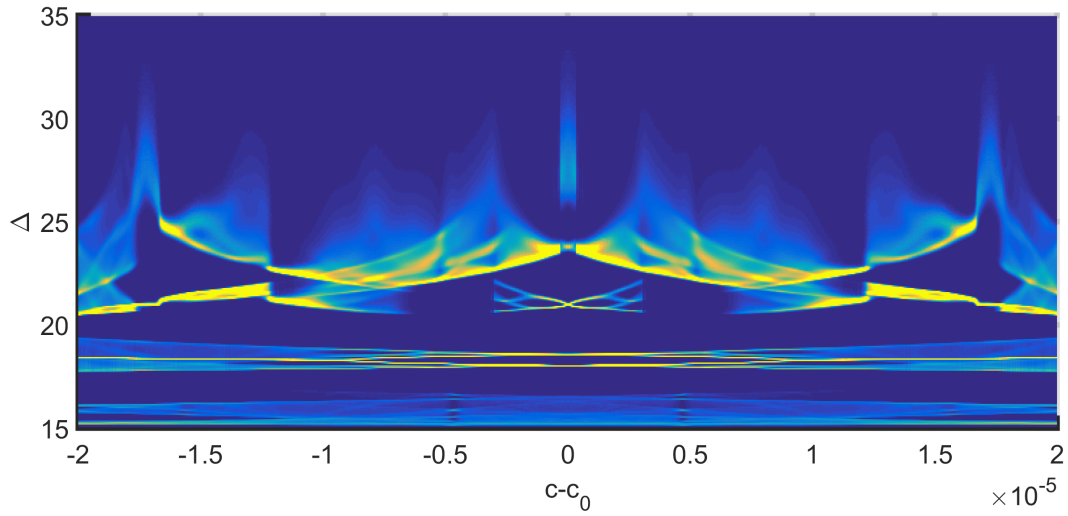
B.2 $\epsilon\sigma = 10^{-8}$

Figure 22: Stationary probability density $\rho_\Delta(\Delta)$ of the timing map (177) for the Shilnikov system for noise strength $\epsilon\sigma = 10^{-8}$. Color from blue to yellow represents low to high values. Scale is arbitrary. White lines show regions plotted in Figures 23 and 24.

Figure 23: Stationary probability density $\rho_\Delta(\Delta)$ of the timing map (177) for the Shilnikov system for noise strength $\epsilon\sigma = 10^{-8}$. Color from blue to yellow represents low to high values. Scale is arbitrary. White lines show region plotted in Figure 24.
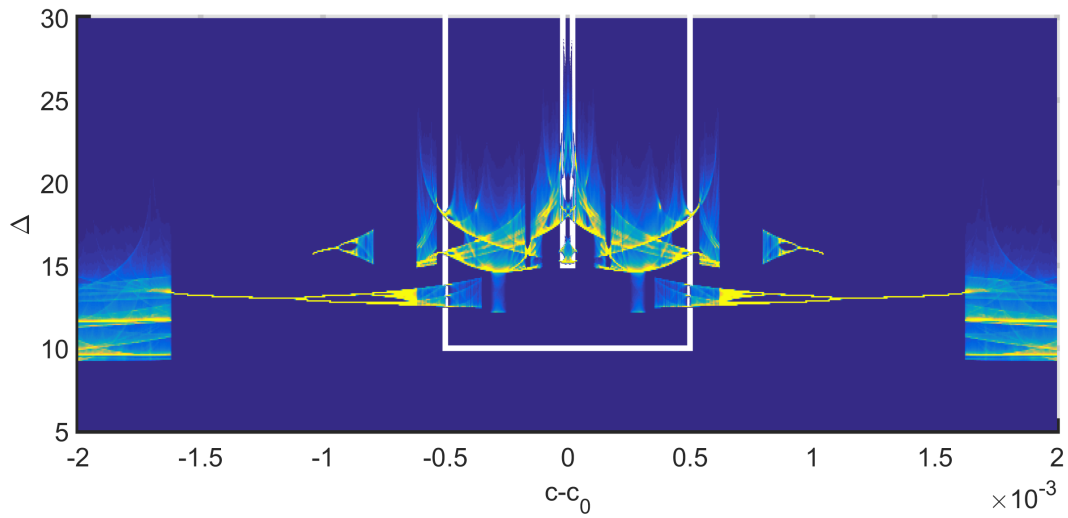

Figure 24: Stationary probability density $\rho_\Delta(\Delta)$ of the timing map (177) for the Shilnikov system for noise strength $\epsilon\sigma = 10^{-8}$. Color from blue to yellow represents low to high values. Scale is arbitrary.
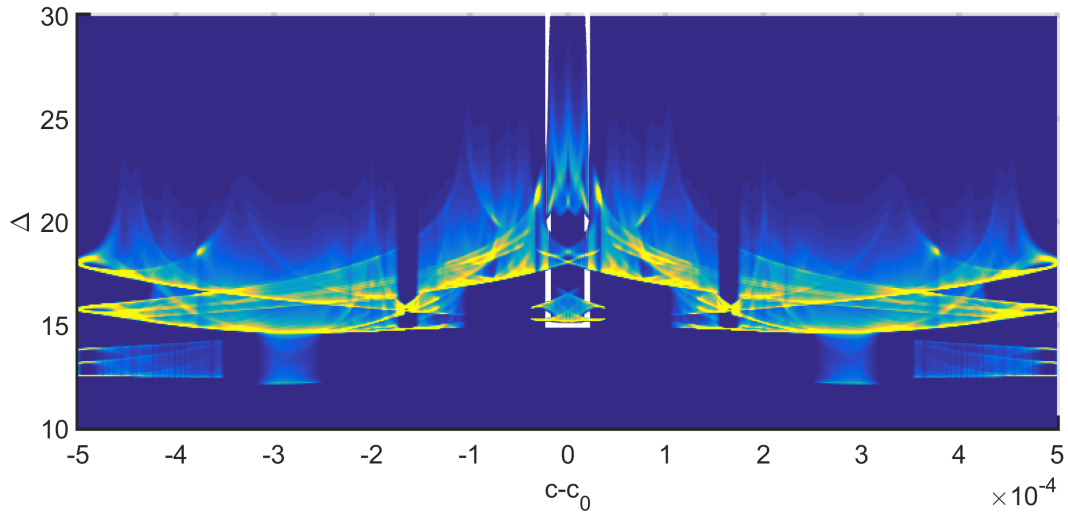
B.3 $\epsilon\sigma = 10^{-7}$

Figure 25: Stationary probability density $\rho_\Delta(\Delta)$ of the timing map (177) for the Shilnikov system for noise strength $\epsilon\sigma = 10^{-7}$. Color from blue to yellow represents low to high values. Scale is arbitrary. White lines show regions plotted in Figures 26 and 27.

Figure 26: Stationary probability density $\rho_\Delta(\Delta)$ of the timing map (177) for the Shilnikov system for noise strength $\epsilon\sigma = 10^{-7}$. Color from blue to yellow represents low to high values. Scale is arbitrary. White lines show region plotted in Figure 27.
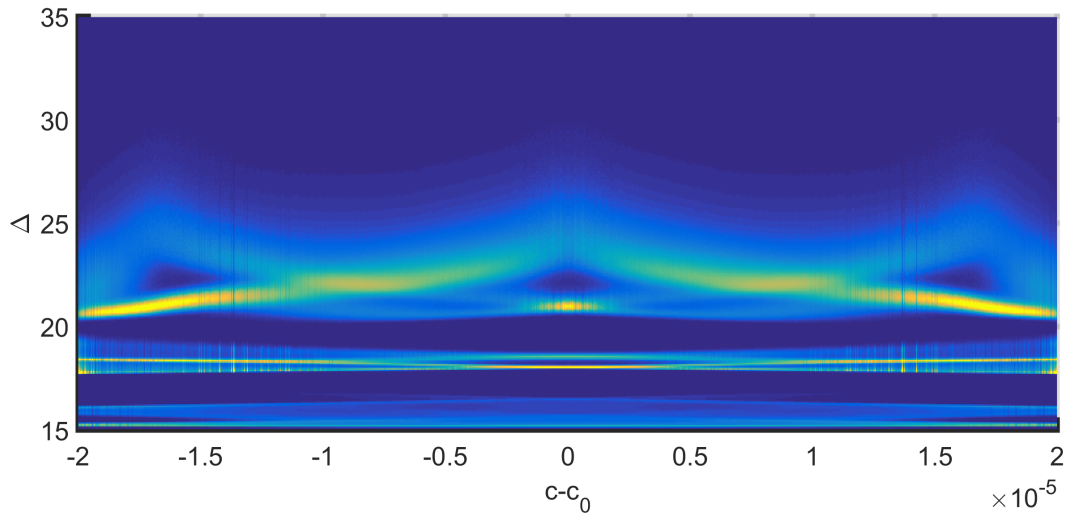
Figure 27: Stationary probability density $\rho_\Delta(\Delta)$ of the timing map (177) for the Shilnikov system for noise strength $\epsilon\sigma = 10^{-7}$. Color from blue to yellow represents low to high values. Scale is arbitrary.
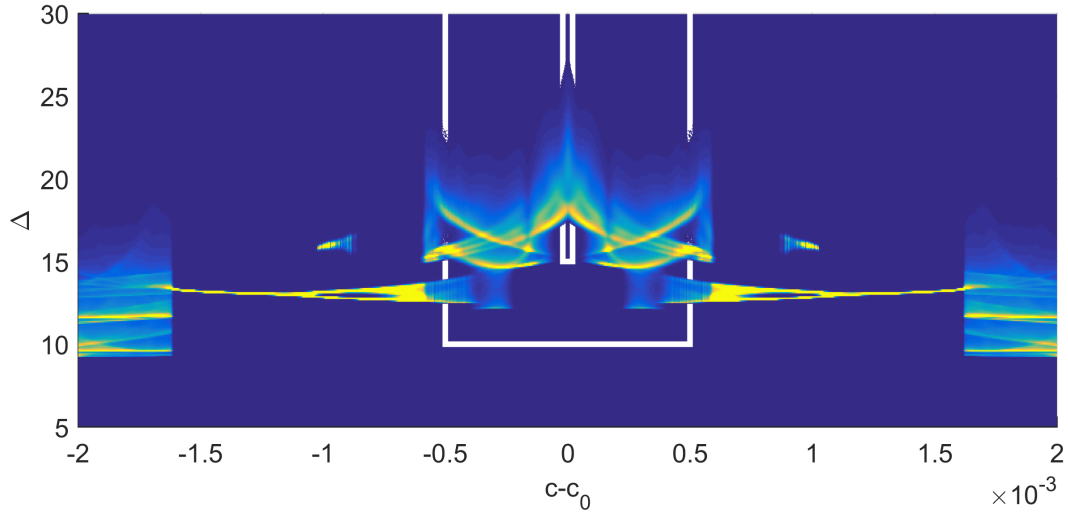
B.4 $\epsilon\sigma = 10^{-6}$

Figure 28: Stationary probability density $\rho_\Delta(\Delta)$ of the timing map (177) for the Shilnikov system for noise strength $\epsilon\sigma = 10^{-6}$. Color from blue to yellow represents low to high values. Scale is arbitrary. White lines show regions plotted in Figures 29 and 30.

Figure 29: Stationary probability density $\rho_\Delta(\Delta)$ of the timing map (177) for the Shilnikov system for noise strength $\epsilon\sigma = 10^{-6}$. Color from blue to yellow represents low to high values. Scale is arbitrary. White lines show region plotted in Figure 30.
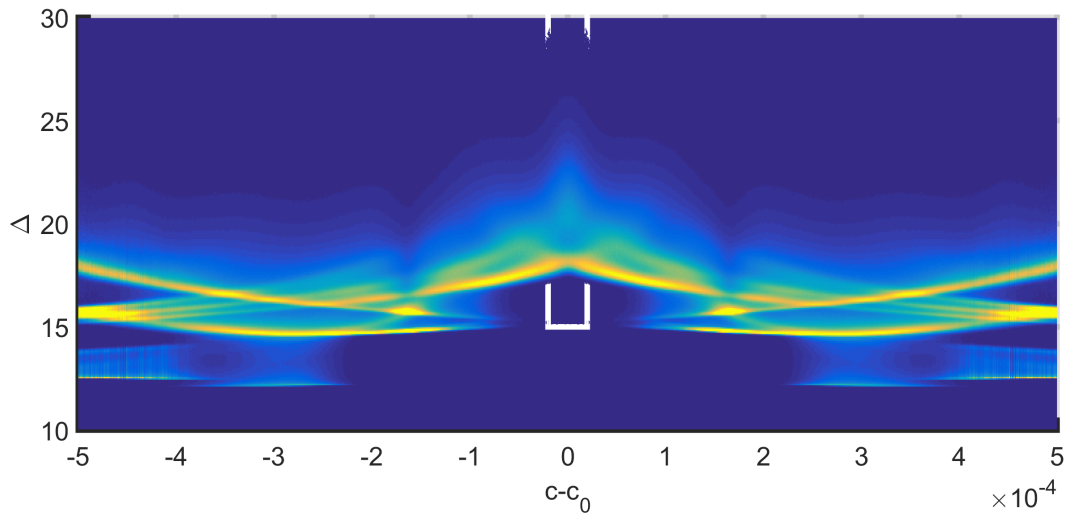

Figure 30: Stationary probability density $\rho_\Delta(\Delta)$ of the timing map (177) for the Shilnikov system for noise strength $\epsilon\sigma = 10^{-6}$. Color from blue to yellow represents low to high values. Scale is arbitrary.
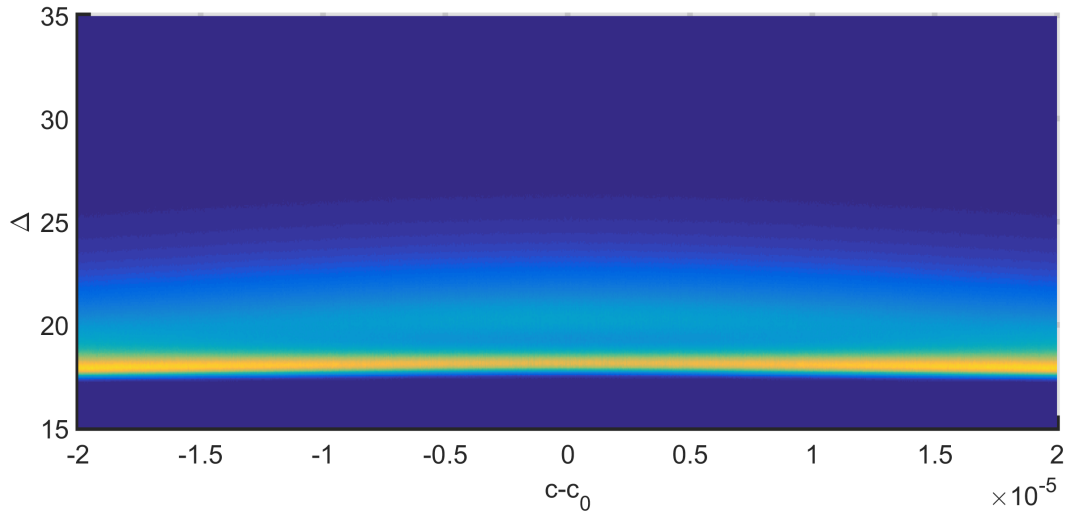
B.5 $\epsilon\sigma = 10^{-5}$

Figure 31: Stationary probability density $\rho_\Delta(\Delta)$ of the timing map (177) for the Shilnikov system for noise strength $\epsilon\sigma = 10^{-5}$. Color from blue to yellow represents low to high values. Scale is arbitrary. White lines show regions plotted in Figures 32 and 33.

Figure 32: Stationary probability density $\rho_\Delta(\Delta)$ of the timing map (177) for the Shilnikov system for noise strength $\epsilon\sigma = 10^{-5}$. Color from blue to yellow represents low to high values. Scale is arbitrary. White lines show region plotted in Figure 33.

Figure 33: Stationary probability density $\rho_\Delta(\Delta)$ of the timing map (177) for the Shilnikov system for noise strength $\epsilon\sigma = 10^{-5}$. Color from blue to yellow represents low to high values. Scale is arbitrary.
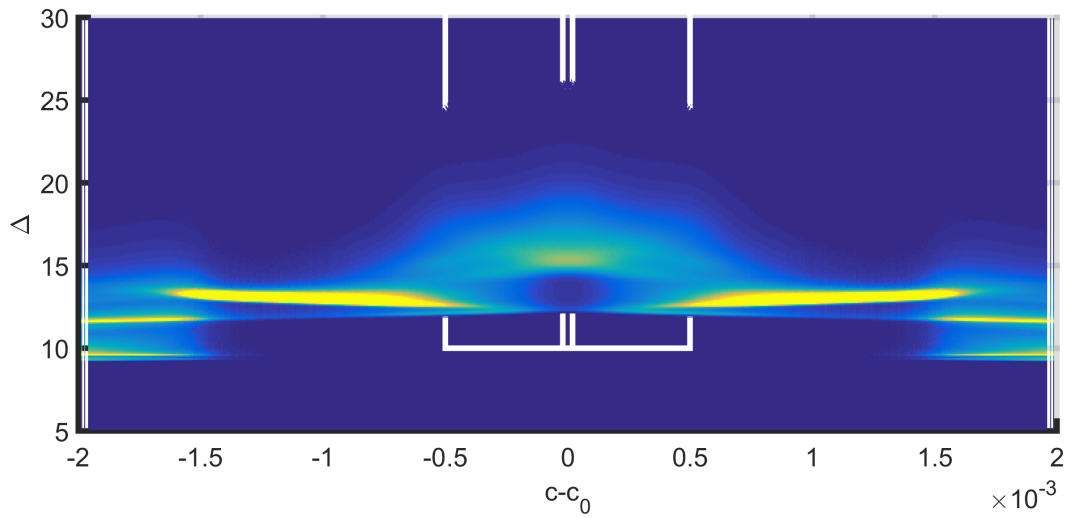
B.6 $\epsilon\sigma = 10^{-4}$

Figure 34: Stationary probability density $\rho_\Delta(\Delta)$ of the timing map (177) for the Shilnikov system for noise strength $\epsilon\sigma = 10^{-4}$. Color from blue to yellow represents low to high values. Scale is arbitrary. White lines show regions plotted in Figures 35 and 36.
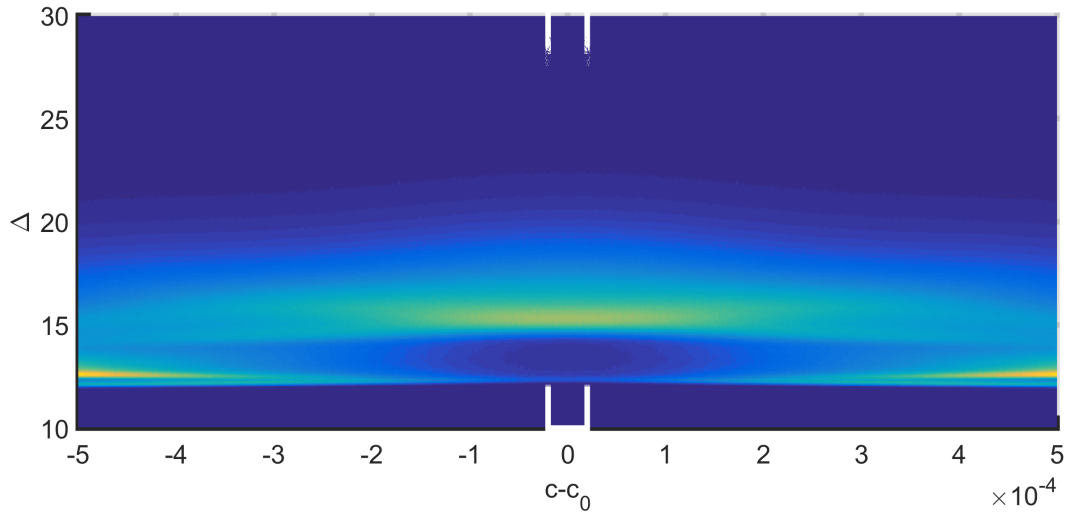
Figure 35: Stationary probability density $\rho_\Delta(\Delta)$ of the timing map (177) for the Shilnikov system for noise strength $\epsilon\sigma = 10^{-4}$. Color from blue to yellow represents low to high values. Scale is arbitrary. White lines show region plotted in Figure 36.
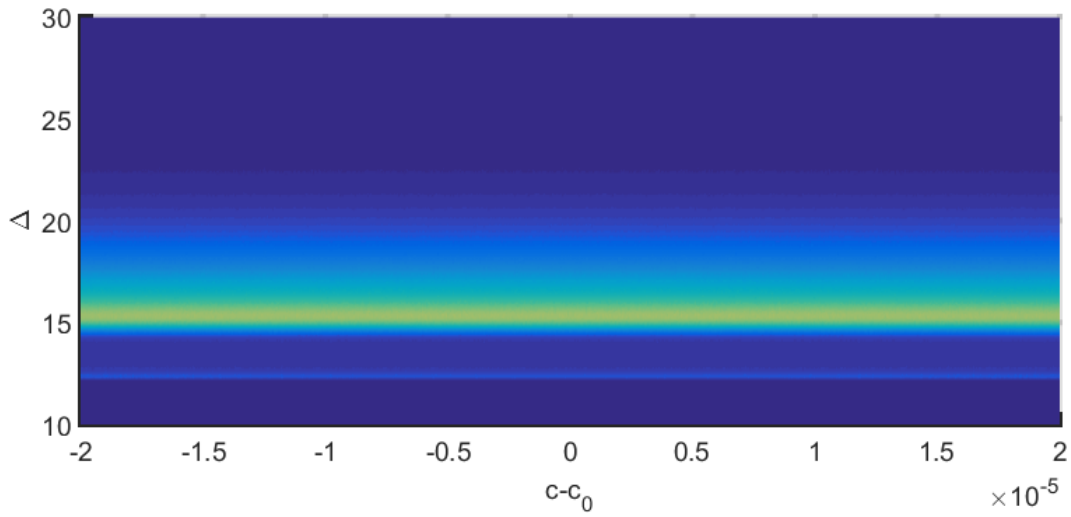

Figure 36: Stationary probability density $\rho_\Delta(\Delta)$ of the timing map (177) for the Shilnikov system for noise strength $\epsilon\sigma = 10^{-4}$. Color from blue to yellow represents low to high values. Scale is arbitrary.